Continuum Mech. Thermodyn. (2009) 21:467–493
DOI 10.1007/s00161-009-0125-1

ORIGINAL ARTICLE

**Clinton P. T. Groth · James G. McDonald**

# Towards physically realizable and hyperbolic moment closures for kinetic theory

Received: 1 May 2009 / Accepted: 6 October 2009 / Published online: 28 November 2009


**Abstract** The numerical prediction of continuum and non-equilibrium flows by using fully hyperbolic and realizable mathematical descriptions that follow from moment closures of gas kinetic theory is reviewed. A brief review is first given of some of the current capabilities and limitations of moment closures for predicting a range of continuum and non-equilibrium flow. Next, an extended but hyperbolic Gaussian closure for diatomic gases that does not account for heat-transfer effects, as well as a regularized version of this closure that incorporates anisotropic thermal-diffusion effects via the inclusion of higher order terms having an elliptic nature, are both reviewed and applied to a number of canonical flow problems. The numerical results for the Gaussian closures clearly demonstrate the capabilities and potential of moment closures and purely hyperbolic treatments. Following these reviews, a somewhat novel hierarchy of physically realizable and hyperbolic moment closures is considered and described. This alternative hierarchy is based on modifications to the more common maximum-entropy hierarchies, so as to ensure the validity and integrability of the approximate distribution function for all values of the velocity moments that are physically realizable. The predictive capabilities of this new closure hierarchy are then explored by considering numerical solutions of the closures for a one-dimensional kinetic equation with a relaxation-time collision operator and by comparing the closure solutions to discrete numerical solutions of this simplified kinetic equation. The study concludes with a brief summary of the findings and a discussion of the potential of the physically realizable and hyperbolic moment closures for application to fully three-dimensional physics.

**Keywords** Gas kinetic theory · Moment closures · Physically realizable moments · Hyperbolic moment equations

**PACS** 47.45.Ab · 47.61.Cb · 47.11.Df

## 1 Introduction

### 1.1 Non-equilibrium micro-scale flows and moment closures

Accurate and reliable numerical methods and mathematical descriptions are required for non-equilibrium micro-scale flows, such as those encountered in the complex conduits of micro-electro-mechanical systems (MEMS) and flows associated with chemical-vapor deposition (CVD) processes commonly encountered in the

Communicated by M. Torrilhon.

C. P. T. Groth (✉), J. G. McDonald
University of Toronto Institute for Aerospace Studies, 4925 Dufferin Street, Toronto, ON M3H 5T6, Canada
E-mail: groth@utias.utoronto.ca

J. G. McDonald
E-mail: mcdonald@utias.utoronto.ca

manufacturing of semiconductor devices [1,2]. In many instances, Knudsen numbers, $Kn$, between 0.01 and 10 are possible for these flows, even at or above atmospheric pressures, and thermal non-equilibrium effects can significantly influence momentum and heat transfer. Nevertheless, computationally tractable mathematical descriptions of non-equilibrium and/or rarefied gaseous flows still remain somewhat illusive. Particle-simulation techniques, such as the direct-simulation Monte Carlo (DSMC) method of Bird [3], and techniques based on the direct discretization of the kinetic equation, such as the approach proposed by Mieussens [4], have been developed for the prediction of general non-equilibrium gaseous flows. However, for near-continuum through to transitional-regime flows, the computational costs incurred by these techniques are considerable. This is particularly true for flows with low Mach numbers and, in these situations, computational expense and storage requirements have prohibited their widespread usage [5,6].

Moment closures offer an approach for handling transition-regime flows ($0.01 \leq Kn \leq 10$) and seem particularly well suited for the treatment of non-equilibrium micro-scale flows [7–10]. For high-speed flows, such as those encountered in hypersonic re-entry to planetary atmospheres, the discontinuous nature (inviscid jumps) provided by moment closures for the predicted internal structure of shocks may be somewhat undesirable [9,11,12]; however, for subsonic and possibly even transonic micro-scale flows, moment closures may offer advantages over other approaches. The computational costs associated with the solution of the partial differential equations (PDEs) governing the time evolution of the moments representing macroscopic quantities of interest in three-dimensional physical space is anticipated to be considerably less than those associated with particle-simulation or direct-discretization solution methods, even for relatively high numbers of moments. Moreover, when seeking solutions of the closures via numerical methods, the purely hyperbolic nature of the resulting moment equations makes them particularly appealing. The hyperbolic moment equations involve only first-order derivatives (this is in contrast to other transport equations that have an elliptic nature and require the evaluation of second- and/or higher order derivatives) and are, therefore, very well suited to solution by the class of very successful Godunov-type finite-volume schemes, which make use of adaptive mesh refinement (AMR) combined with treatments for embedded and moving boundaries and interfaces [13–18]. For hyperbolic systems, schemes of this type are robust, insensitive to irregularities in the computational grids, minimize discretization errors, provide accurate resolution of discontinuities, and permit the systematic application of physically realistic boundary conditions. When coupled with AMR, they permit treatment of complex and evolving flow geometries and the resolution of highly disparate length scales while, at the same time, optimizing the usage of computational resources. They also have narrow stencils, making them suitable for implementation on massively parallel computer architectures [14–18].

Unfortunately, moment closures are not without their limitations. Although the original closure hierarchies due to Grad [7] result in moment equations that are hyperbolic for near-equilibrium flows, these PDEs can suffer from closure breakdown and loss of hyperbolicity, even for relatively small departures from equilibrium conditions and for what are certainly physically realistic or realizable sets of macroscopic moments. Closure breakdown in this case refers specifically to the invalidness of the moment closures for initial value problems due to the loss of hyperbolicity. The term is also used herein more generally to refer to the failure and/or invalidity of closures for reasons ranging from loss of hyperbolicity to non-integrability of the distribution function. Moment realizability refers here to the existence of a positive semi-definite velocity distribution function corresponding to the set of predicted velocity moments and is formally defined in Sect. 2.2.

The Grad closures are based on truncated polynomial series expansions for the velocity distribution function in terms of the well-known equilibrium Maxwellian distribution. They do not, therefore, enforce positivity of this approximate solution for the non-equilibrium distribution function, and, for significant departures from equilibrium, the regions of non-positivity of the distribution function in velocity space result in closure breakdown and non-hyperbolicity of the moment equations. More recently, Struchtrup and Torrilhon [10,19–21] have proposed regularized variants of the Grad moment closure hierarchy based on a Chapman–Enskog expansion technique applied directly to the moment equations. Although the regularized closures have proved to be quite promising and result in smooth transitions for shocks (a desirable feature for high-speed applications, such as re-entry flows), the resulting transport equations for the moments are of mixed type (i.e., the moment fluxes are functions of the velocity moments and their derivatives) and formal hyperbolicity of the closures is lost. As a consequence, the computational advantages of purely hyperbolic treatments discussed above are also lost and one is faced with dealing with the challenges associated with the discretization of higher order derivatives of the solution on irregular meshes, for which there can be serious trade-offs between accuracy and positivity (related to the satisfaction of the maximum principal) of the spatial discretization operator [22,23]. Both accurate and positive discretizations of the Laplacian operator can be difficult to achieve on computational mesh having large variations in the sizes of adjacent cells as can typically occur in AMR techniques. Additionally,

the regularization process does not avoid the issues associated with closure breakdown and non-realizability of the predicted moments.

Alternative moment-closure techniques have been proposed based on the assumption that the approximate form for the distribution function corresponds to that of the maximum-entropy distribution [8,9]. The maximum-entropy distribution is defined to be the distribution that maximizes the entropy subject to the constraint that it be consistent with a given finite set of velocity moments. Non-negative values for the approximate form of the distribution function can be assured through the judicious selection of closure moments. More importantly, moment closures obtained in this manner can be imbued with many desirable mathematical properties including hyperbolicity, realizability of moments, and a definable entropy relation [8]. Based on these ideas, Levermore [8] has proposed a hierarchy of maximum-entropy closures. The lowest order members of this hierarchy are the Mawellian and Gaussian closures, both of which yield strictly hyperbolic moment equations and physically realizable moments. Numerical solutions of the Gaussian closure using Godunov-type finite-volume schemes have been considered by Brown et al. [11,12] and McDonald and Groth [14,24] and illustrate some of the computational advantages of having a strictly hyperbolic and physically realizable treatment (further evidence will be provided herein). Unfortunately, high-order members of Levermore hierarchy (those closures containing super-quadratic velocity moments) do not remain valid for the full range of physically realizable moments. As shown by Junk and co-workers [25–28], the entropy maximization problem is not guaranteed to have a solution for all physically realizable velocity moments. This deleterious result is in fact true for any high-order maximum-entropy closures and is particularly devastating as local equilibrium solutions can be shown to lie on the boundary in moment space separating the valid region for the closure, in which the entropy maximization problem can be solved, from the invalid region, in which a solution to the entropy maximization problem cannot be found [26]. Obviously, this situation is not tenable for practical computations of non-equilibrium gaseous flows and has prevented the wider application of maximum-entropy-based moment closures.

### 1.2 Scope of current study

This study is then concerned with the development of moment closures, which remain both physically realizable and strictly hyperbolic for the full range of velocity moments. It is felt that closures with these mathematical properties would be much more robust and reliable for practical applications. Following a brief overview of moment-closure techniques, the potential of hyperbolic and realizable closures for describing both continuum and non-equilibrium micro-scale flows is first demonstrated by reviewing the predictive capabilities of the Gaussian closure (a low-order member of the Levermore hierarchy). In particular, an extended but hyperbolic Gaussian closure for diatomic gases that does not account for heat-transfer effects, as well as a regularized version of this closure that incorporates anisotropic thermal-diffusion effects via the inclusion of higher order terms having an elliptic nature, are both reviewed and applied to a number of canonical flow problems. The potential of moment closures and benefits of a purely hyperbolic treatment are demonstrated. Following this review, a somewhat novel hierarchy of physically realizable and hyperbolic moment closures is considered and described. This alternative hierarchy is based on modifications to the maximum-entropy hierarchy of Levermore so as to ensure the validity and integrability of the approximate distribution function for all values of the velocity moments that are physically realizable. The predictive capabilities of this new closure hierarchy are then explored by considering numerical solutions of the closures for a one-dimensional kinetic equation with a relaxation-time collision operator and by comparing the closure solutions to discrete numerical solutions of this simplified kinetic equation. The article concludes with a brief summary of the findings and a discussion of the potential of the proposed physically realizable and hyperbolic moment closures for application to fully three-dimensional physics.

## 2 Moment closures

### 2.1 Kinetic theory and Boltzmann equation

In order to effectively treat non-equilibrium flows, the particle nature of fluids must be considered. This is accomplished in classical gas kinetic theory by adopting a statistical treatment. A probability density function, $\mathcal{F}(\vec{x}, \vec{v}, t)$, is defined in six-dimensional phase space, which specifies the probability of finding particles at a

given location, $\vec{x}$, and time, $t$, having a particular gas velocity, $\vec{v}$. Macroscopic moments or "observable" properties, $M(\vec{x}, t)$, of the gas are then obtained by taking appropriate velocity moments of $\mathcal{F}$, i.e., by integrating the product of an appropriate velocity-dependent weight, $V(\vec{v})$, and the distribution function over all velocity space:

$$M(\vec{x}, t) = \langle V(\vec{v})\mathcal{F}\rangle = \int_{-\infty}^{\infty}\int_{-\infty}^{\infty}\int_{-\infty}^{\infty} V(\vec{v})\mathcal{F}(\vec{x}, \vec{v}, t)d^3v. \tag{1}$$

For example $\rho = m\langle\mathcal{F}\rangle$, $\rho\vec{u} = m\langle\vec{v}\mathcal{F}\rangle$, and $\vec{\vec{P}} = m\langle\vec{c}\vec{c}\mathcal{F}\rangle$. Here $m$ is the mass of a particle, $\rho$ the gas density, $\vec{u}$ the average or bulk velocity of the gas, $\vec{c} = \vec{v} - \vec{u}$ the random velocity of the particles, and $\vec{\vec{P}}$ the generalized pressure dyad with $\vec{\vec{P}} = \vec{\vec{I}}p - \vec{\vec{\tau}}$ and $p$ and $\vec{\vec{\tau}}$ the pressure and fluid stress dyad, respectively.

The time evolution of the velocity distribution function, $\mathcal{F}$, is given by the Boltzmann equation [9,10,29,30]. This is an integro-differential equation given by

$$\frac{\partial\mathcal{F}}{\partial t} + \vec{v}\cdot\vec{\nabla}\mathcal{F} = \frac{\delta\mathcal{F}}{\delta t}, \tag{2}$$

where $\delta\mathcal{F}/\delta t$, is the Boltzmann collision operator representing the time rate of change of the distribution function produced by inter-particle collisions. Transport equations governing the time evolution of the macroscopic quantities can be derived by evaluating velocity moments of the Boltzmann equation. Given a set of $N$ velocity weights of interest, $\mathbf{V}^{(N)}$, given by

$$\mathbf{V}^{(N)} = m[1, \vec{v}, \vec{v}\vec{v}, v^2, \ldots]^{\mathrm{T}}, \tag{3}$$

and the corresponding moments, $\mathbf{M}^{(N)}$, with

$$\mathbf{M}^{(N)} = \int_{-\infty}^{\infty}\int_{-\infty}^{\infty}\int_{-\infty}^{\infty} \mathbf{V}^{(N)}\mathcal{F}(\vec{x}, \vec{v}, t)d^3v = \left\langle\mathbf{V}^{(N)}\mathcal{F}\right\rangle, \tag{4}$$

evaluation of the corresponding velocity moments of the Boltzmann equation above leads to Maxwell's equation of change for the moments, $\mathbf{M}^{(N)}$, given by

$$\frac{\partial}{\partial t}\left(\mathbf{M}^{(N)}\right) + \vec{\nabla}\cdot\left\langle\vec{v}\,\mathbf{V}^{(N)}\mathcal{F}\right\rangle = \left\langle\mathbf{V}^{(N)}\frac{\delta\mathcal{F}}{\delta t}\right\rangle. \tag{5}$$

The moment equations above can be seen to be a coupled first-order quasi-linear system of PDEs in classical weak conservation form (divergence form with sources and/or sinks) having relaxation (source) terms, $\left\langle\mathbf{V}^{(N)}\delta\mathcal{F}/\delta t\right\rangle$, that represent the time rate of change of the velocity moments produced by particle collisions.

## 2.2 Realizability of velocity moments

For a given set of velocity moments, $\mathbf{M}^{(N)}$, realizability deals with the issue of whether or not the velocity moments correspond to those of a physically plausible, positive semi-definite, phase-space distribution function. Although a finite set of velocity moments cannot be used to uniquely specify a distribution function and multiple distributions can be defined, which share the same $N$ moment densities, in assessing moment realizability, the question is asked whether a positive-valued distribution function can give rise to the given set of moments. For a given set of velocity weights, $\mathbf{V}^{(N)} = m[1, \vec{v}, \vec{v}\vec{v}, v^2, \ldots]^{\mathrm{T}}$, and moments, $\mathbf{M}^{(N)} = m\left\langle\mathbf{V}^{(N)}\mathcal{F}\right\rangle$, one can construct polynomials, $\mathcal{P}^{(N)}(\vec{v})$, with

$$\mathcal{P}^{(N)}(\vec{v}) = \boldsymbol{\alpha}^{\mathrm{T}}\mathbf{V}^{(N)}, \tag{6}$$

where $\boldsymbol{\alpha}^{\mathrm{T}}$ are the coefficients of the polynomial. For any positive-valued distribution, $\mathcal{F}$, and polynomial, $\mathcal{P}^{(N)}$, it is clearly a requirement that

$$\left\langle||\mathcal{P}^{(N)}(\vec{v})||^2\mathcal{F}\right\rangle = \boldsymbol{\alpha}^{\mathrm{T}}\left\langle\mathbf{V}^{(N)}\left[\mathbf{V}^{(N)}\right]^{\mathrm{T}}\mathcal{F}\right\rangle\boldsymbol{\alpha} = \boldsymbol{\alpha}^{\mathrm{T}}\mathbf{H}^{(N)}\boldsymbol{\alpha} \geq 0, \tag{7}$$

and thus the moments, $\mathbf{M}^{(N)}$, are realizable provided the real symmetric matrix, $\mathbf{H}^{(N)}$, given by

$$\mathbf{H}^{(N)} = \left\langle \mathbf{V}^{(N)} \left[ \mathbf{V}^{(N)} \right]^{\mathrm{T}} \mathcal{F} \right\rangle, \tag{8}$$

is positive definite. For situations in which $\mathbf{H}^{(N)}$ is non-positive definite, it follows that the velocity moments are not consistent with any possible positive-valued distribution function and, hence, are not physically realizable. The preceding analysis for moment realizability follows from the early work of Hamburger [31,32] and is closely related to the now classical Hamburger moment problem.

### 2.3 Grad closure hierarchy

The problem of closure can be seen by returning to the moment equations of Eq. (5). It is quite apparent that the time evolution of the moments, $\mathbf{M}^{(N)}$, is dependent on the divergence of the moment fluxes, $\langle \vec{v}\, \mathbf{V}^{(N)} \mathcal{F} \rangle$. The latter includes moments of one higher order in terms of the velocity, $\vec{v}$. Consequently, the time evolution of every moment is dependent on a moment of one higher order in $\vec{v}$ and, in general, an infinite number of moment equations is required to fully describe the evolution of any given macroscopic flow quantity. Solution of this infinite system is equivalent to solving Eq. (2).

One technique for obtaining a closed system of moment equations and thereby arriving at an approximate solution for the Boltzmann equation is to restrict the distribution function to some assumed form [7]. Restricting the form of the distribution function has the effect of restricting the value of higher order velocity moments to be functions of lower order moments, thus providing a closing relationship. Perhaps, the most well-known assumed form for the distribution function is the Grad-type polynomial series expansions having the form [7]

$$\mathcal{F}^{(N)} = \mathcal{M} \left[ 1 + \mathcal{P}^{(N)}(\vec{c}) \right] = \left[ 1 + \boldsymbol{\alpha}^{\mathrm{T}} \mathbf{C}^{(N)} \right], \tag{9}$$

where the expansion is performed about the equilibrium solution or Maxwellian distribution function, $\mathcal{M}$, given by

$$\mathcal{M} = \frac{\rho}{m\,(2\pi p/\rho)^{3/2}} \exp\left( -\frac{1}{2} \frac{\rho c^2}{p} \right), \tag{10}$$

and $\mathcal{P}^{(N)}(\vec{c}) = \boldsymbol{\alpha}^{\mathrm{T}} \mathbf{C}^{(N)}$ for which $\mathbf{C}^{(N)}$ are the finite set of velocity weights of interest in terms of the random particle velocity. The $N$ random-velocity moments of interest satisfy

$$\mathbf{M}^{(N)}(\mathbf{C}^{(N)}) = \left\langle \mathbf{C}^{(N)} \mathcal{F}^{(N)} \right\rangle, \tag{11}$$

and $\boldsymbol{\alpha}$ are the coefficients of the expansion. They may be related to the velocity moments by satisfying the conditions imposed on the expansion for $\mathcal{F}^{(N)}$ given by Eq. (11). In the original work of Grad [7], both 13- and 20-moment closures were considered with

$$N = 13, \quad \mathbf{C}^{(13)} = [1, c_i, c_i c_j, c_i c^2/2]^{\mathrm{T}}, \quad \mathbf{M}^{(13)} = [\rho, \rho u_i, P_{ij}, q_i]^{\mathrm{T}}, \tag{12}$$

and

$$N = 20, \quad \mathbf{C}^{(20)} = [1, c_i, c_i c_j, c_i c_j c_k]^{\mathrm{T}}, \quad \mathbf{M}^{(20)} = [\rho, \rho u_i, P_{ij}, Q_{ijk}]^{\mathrm{T}}, \tag{13}$$

respectively, where $q_i$ and $Q_{ijk}$ are the heat-flux vector and generalized heat-flux tensor. Extensions to many more moments has since been considered by other researchers [9,10]. It is generally assumed that the inclusion of more moments in a closure leads to a greater possibility that the resulting approximate distribution can more closely approximate general non-equilibrium behaviour.

Although Grad-type expansions result in a closed set of hyperbolic transport equations for a finite set of velocity moments, the assumed distribution function can in many cases be non-physical. It is possible for Eq. (9) to yield negative probabilities for some values of the particle velocity. This is particularly true in the tails of the distribution function for large random velocities. More significantly, this non-positivity of the approximate form for the distribution function can result in closure breakdown and non-hyperbolicity of the moment equations for physically realizable moments not too far removed from near equilibrium conditions. As a consequence, the moment equations become ill-posed for initial-value problems, a property that is obviously highly undesirable.

### 2.4 Levermore maximum-entropy closure hierarchy

An alternate technique for selecting an assumed form for the distribution function is to choose the function which maximizes the entropy for a given finite set of moments [8–10]. This technique yields distribution functions of the form

$$\mathcal{F}^{(N)} = \exp\left(\mathcal{P}^{(N)}(\vec{c})\right) = \exp\left(\boldsymbol{\alpha}^{\mathrm{T}}\mathbf{C}^{(N)}\right), \tag{14}$$

where again $\mathbf{C}^{(N)}$ are the finite set of velocity weights of interest corresponding to the moments $\mathbf{M}^{(N)} = \left\langle \mathbf{C}^{(N)}\mathcal{F}^{(N)}\right\rangle$, and $\boldsymbol{\alpha}$ is a vector of closure coefficients which depend on the local macroscopic quantities, $\mathbf{M}^{(N)}$. Unlike the series expansions of Grad, which can be viewed as perturbative expansions about the Maxwellian, this exponential form for the distribution function is non-perturbative and strictly positive-valued while remaining finite even as $|\vec{c}| \to \infty$ through the careful selection of the vector of velocity weights, $\mathbf{C}^{(N)}$.

Levermore [8] has proposed a hierarchy of maximum-entropy closures with many desirable mathematical properties, including a positive-valued distribution function, hyperbolic moments equations, realizability of predicted moments, and a definable entropy relation. The Levermore hierarchy included 5-, 10-, 14-, 21-, 26-, and 35-moment closures with

$$N = 5, \quad \mathbf{C}^{(5)} = m[1, c_i, c^2/2]^{\mathrm{T}}, \quad \mathbf{M}^{(5)} = [\rho, \rho u_i, p]^{\mathrm{T}}, \tag{15}$$

$$N = 10, \quad \mathbf{C}^{(10)} = m[1, c_i, c_i c_j]^{\mathrm{T}}, \quad \mathbf{M}^{(10)} = [\rho, \rho u_i, P_{ij}]^{\mathrm{T}}, \tag{16}$$

$$N = 14, \quad \mathbf{C}^{(14)} = m[1, c_i, c_i c_j, c_i c^2/2, c^4/15]^{\mathrm{T}}, \quad \mathbf{M}^{(14)} = [\rho, \rho u_i, P_{ij}, q_i, r]^{\mathrm{T}}, \tag{17}$$

$$N = 21, \quad \mathbf{C}^{(21)} = m[1, c_i, c_i c_j, c_i c_j c_k, c^4/15]^{\mathrm{T}}, \quad \mathbf{M}^{(21)} = [\rho, \rho u_i, P_{ij}, Q_{ijk}, r]^{\mathrm{T}}, \tag{18}$$

$$N = 26, \quad \mathbf{C}^{(26)} = m[1, c_i, c_i c_j, c_i c_j c_k, c_i c_j c^2]^{\mathrm{T}}, \quad \mathbf{M}^{(26)} = [\rho, \rho u_i, P_{ij}, Q_{ijk}, r_{ij}]^{\mathrm{T}}, \tag{19}$$

$$N = 35, \quad \mathbf{C}^{(35)} = m[1, c_i, c_i c_j, c_i c_j c_k, c_i c_j c_k c_l]^{\mathrm{T}}, \quad \mathbf{M}^{(35)} = [\rho, \rho u_i, P_{ij}, Q_{ijk}, R_{ijkl}]^{\mathrm{T}}, \tag{20}$$

where $R_{ijkl} = m\left\langle c_i c_j c_k c_l \mathcal{F}\right\rangle$ is the generalized fourth-order velocity moment tensor, $r_{ij} = R_{ijkk}$, and $r = R_{iikk}/15$. Provided that the maximum entropy distribution of Eq. (14) is definable, Levermore [8] has demonstrated the hyperbolicity of the resulting moment equations. By defining the density and flux potentials, $h(\boldsymbol{\alpha})$ and $\vec{f}(\boldsymbol{\alpha})$ given by

$$h(\boldsymbol{\alpha}) = \left\langle e^{\boldsymbol{\alpha}^{\mathrm{T}}\mathbf{V}^{(N)}}\right\rangle, \quad \vec{f}(\boldsymbol{\alpha}) = \left\langle \vec{v} e^{\boldsymbol{\alpha}^{\mathrm{T}}\mathbf{V}^{(N)}}\right\rangle, \tag{21}$$

the closure moments and moment fluxes can be expressed simply as

$$h_{\boldsymbol{\alpha}} = \frac{\partial h}{\partial \boldsymbol{\alpha}} = \left\langle \mathbf{V}^{(N)} e^{\boldsymbol{\alpha}^{\mathrm{T}}\mathbf{V}^{(N)}}\right\rangle, \quad \vec{f}_{\boldsymbol{\alpha}} = \frac{\partial \vec{f}}{\partial \boldsymbol{\alpha}} = \left\langle \vec{v}\, \mathbf{V}^{(N)} e^{\boldsymbol{\alpha}^{\mathrm{T}}\mathbf{V}^{(N)}}\right\rangle \tag{22}$$

and the moment equations of Eq. (5) can then be written as

$$\frac{\partial}{\partial t}(h_{\boldsymbol{\alpha}}) + \vec{\nabla}\cdot\vec{f}_{\boldsymbol{\alpha}} = \left\langle \mathbf{V}^{(N)}\frac{\delta\mathcal{F}}{\delta t}\right\rangle = \mathbf{R}(\boldsymbol{\alpha}), \tag{23}$$

where $\mathbf{R}(\boldsymbol{\alpha}) = \left\langle \mathbf{V}^{(N)}\delta\mathcal{F}/\delta t\right\rangle$ is the source term associated with collisional processes. The terms $h_{\alpha}$ and $\vec{f}_{\alpha}$ can be differentiated again to give

$$h_{\boldsymbol{\alpha}\boldsymbol{\alpha}} = \left\langle \mathbf{V}^{(N)}\left[\mathbf{V}^{(N)}\right]^{\mathrm{T}} e^{\boldsymbol{\alpha}^{\mathrm{T}}\mathbf{V}^{(N)}}\right\rangle, \quad \vec{f}_{\boldsymbol{\alpha}\boldsymbol{\alpha}} = \left\langle \vec{v}\, \mathbf{V}^{(N)}\left[\mathbf{V}^{(N)}\right]^{\mathrm{T}} e^{\boldsymbol{\alpha}^{\mathrm{T}}\mathbf{V}^{(N)}}\right\rangle, \tag{24}$$

and the moment equations above can be re-expressed as

$$h_{\boldsymbol{\alpha}\boldsymbol{\alpha}}\frac{\partial \boldsymbol{\alpha}}{\partial t} + \vec{f}_{\boldsymbol{\alpha}\boldsymbol{\alpha}}\cdot\vec{\nabla}\boldsymbol{\alpha} = \mathbf{R}(\boldsymbol{\alpha}). \tag{25}$$

Equation (25) describes the time evolution and transport of the closure coefficients, $\boldsymbol{\alpha}$, for the maximum-entropy distribution. Hyperbolicity of this system is assured by the symmetry of $\vec{f}_{\alpha\alpha}$ and symmetric positive definiteness of $h_{\alpha\alpha}$. Note that for any weighting coefficients, $\mathbf{w}$,

$$\mathbf{w}^{\mathrm{T}}h_{\boldsymbol{\alpha}\boldsymbol{\alpha}}\mathbf{w} = \left\langle \mathbf{w}^{\mathrm{T}}\mathbf{V}^{(N)}\left[\mathbf{V}^{(N)}\right]^{\mathrm{T}}\mathbf{w}\; e^{\boldsymbol{\alpha}^{\mathrm{T}}\mathbf{V}^{(N)}}\right\rangle \geq 0 \tag{26}$$

and hence $h_{\alpha\alpha}$ is both symmetric and positive definite. The transport equations of Eq. (25) are in the form of a Godunov symmetric hyperbolic system [33] and this form can be shown to be equivalent to the classical Friedrichs–Lax form for hyperbolic systems [8,34].

As first noted by Godunov [33], symmetric hyperbolic systems of the form given in Eq. (25) can be shown to satisfy an additional scalar entropy balance or dissipation law. Multiplication of Eq. (25) by $\boldsymbol{\alpha}^{\mathrm{T}}$ and subsequent manipulation leads to

$$\frac{\partial}{\partial t}\left(\boldsymbol{\alpha}^{\mathrm{T}} h_{\alpha} - h\right) + \vec{\nabla}\cdot\left(\boldsymbol{\alpha}^{\mathrm{T}}\vec{f}_{\alpha} - \vec{f}\right) = \boldsymbol{\alpha}^{\mathrm{T}}\mathbf{R}(\boldsymbol{\alpha}). \tag{27}$$

Defining the entropy function, $s(\mathbf{M}^{(N)})$, to be Legendre transform of the density potential, $h(\boldsymbol{\alpha})$, given by

$$s(\mathbf{M}^{(N)}) + h(\boldsymbol{\alpha}) = \boldsymbol{\alpha}^{\mathrm{T}}\mathbf{M}^{(N)} = \boldsymbol{\alpha}^{\mathrm{T}} h_{\alpha}, \tag{28}$$

and the entropy flux to be Legendre transform of flux potential, $\vec{f}(\boldsymbol{\alpha})$, such that

$$\vec{j}(\mathbf{M}^{(N)}) + \vec{f}(\boldsymbol{\alpha}) = \boldsymbol{\alpha}^{\mathrm{T}}\vec{f}_{\alpha}, \tag{29}$$

then a dissipative entropy balance equation for $s(\mathbf{M}^{(N)})$ can be obtained from Eq. (27) and written as

$$\frac{\partial s}{\partial t} + \vec{\nabla}\cdot\vec{j} = \boldsymbol{\alpha}^{\mathrm{T}}\mathbf{R}(\boldsymbol{\alpha}) = s_{\mathbf{M}}^{\mathrm{T}}\mathbf{R}(s_{\mathbf{M}}), \tag{30}$$

where $s_{\mathbf{M}} = \partial s/\partial \mathbf{M} = \boldsymbol{\alpha}$.

### 2.5 Maximum-entropy distribution

The proof of hyperbolicity and the definition of a dissipative entropy given above are rather elegant and establish a great deal of promise for maximum-entropy moment closures. Nevertheless, the results are predicated on the existence of a maximum-entropy distribution of the form given in Eq. (14), for all physically realizable moments. The distribution function of Eq. (14) is the form that maximizes the physical entropy of the system for a given finite set of $N$ moments, $\mathbf{M}^{(N)}$. This maximization process is equivalent to the minimization of the closure entropy, $s(\mathbf{M}^{(N)})$, defined in Eq. (28) above and often termed the mathematical entropy. Although the maximum-entropy closures could be equally referred to as "minimum-entropy" closures, as they formally correspond to the distribution function having the minimum mathematical entropy for a given set of moments, the more commonly used term "maximum-entropy" is applied herein in reference to the closures' maximization of physical entropy.

Given the values of the moments, $\mathbf{M}^{(N)}$, the entropy, $s(\mathbf{M}^{(N)})$, and closure coefficients, $\boldsymbol{\alpha}$, can be determined via the solution of the minimization problem given by

$$s(\mathbf{M}^{(N)}) = -\min_{\boldsymbol{\alpha}}\left[h(\boldsymbol{\alpha}) - \boldsymbol{\alpha}^{\mathrm{T}}\mathbf{M}^{(N)}\right]. \tag{31}$$

where $h(\boldsymbol{\alpha})$ is differentiable, the solution of this minimization problem satisfies

$$\frac{\partial}{\partial \boldsymbol{\alpha}}\left[h(\boldsymbol{\alpha}) - \boldsymbol{\alpha}^{\mathrm{T}}\mathbf{M}^{(N)}\right] = 0 \tag{32}$$

yielding

$$\mathbf{M}^{(N)} = h_{\alpha} = \left\langle \mathbf{V}^{(N)} e^{\boldsymbol{\alpha}^{\mathrm{T}}\mathbf{V}^{(N)}} \right\rangle. \tag{33}$$

This solution has a mathematical entropy minimum for the given set of moments. The minimization problem above can be used to define a numerical approach for relating $\boldsymbol{\alpha}$ and $\mathbf{M}^{(N)}$ in situations for which explicit analytical expressions relating the coefficients to the predicted moments are not possible.

The $N = 5$ and $N = 10$ lower order closures of the Levermore hierarchy correspond to the Maxwellian and Gaussian closures. In these cases, closed-formed analytical expression relating the closure coefficients, $\boldsymbol{\alpha}$, to the predicted moments, $\mathbf{M}^{(N)}$, can be found and maximum-entropy distributions can be defined for the full range of physically realizable moments. Strict hyperbolicity of the moment equations is also assured

for all realizable moments. For the Maxwellian model, the approximate distribution function is equal to the equilibrium of Maxwellian distribution function, $\mathcal{M}$, defined in Eq. (10) above (i.e., $\mathcal{F}^{(5)} = \mathcal{M}$) and, for the Gaussian model, the distribution function takes the form

$$\mathcal{F}^{(10)} = \mathcal{G} = \frac{\rho}{m(2\pi)^{3/2}(\det \boldsymbol{\Theta})^{1/2}} e^{\left(-\frac{1}{2}\Theta_{ij}^{-1} c_i c_j\right)}, \tag{34}$$

where $\Theta_{ij} = P_{ij}/\rho$ is an anisotropic "temperature" tensor. The Gaussian distribution appears to have been first derived in early work by Maxwell [35] and then re-discovered in subsequent but independent research by both Schlüter [36,37] and Holway [38–41]. It may be regarded as a generalization of the bi- and tri-Maxwellian velocity distribution functions with a form that does not require the identification of the planes of principal stress. This approximate non-equilibrium distribution possesses a Gaussian-like distribution in each of the principal strain axes. Physically, it corresponds to a non-equilibrium condition with a different temperature in each direction.

One potential stumbling block to practical application arises for all closures in the Levermore hierarchy beyond the the Maxwellian and Gaussian systems: a numerical approach is required to relate moments and coefficients of expansion as explicit analytical expressions are not achievable. This can significantly increase the computational costs of carrying out a computation using the high-order maximum-entropy moment closures. However, a much more severe problem also appears for all closures beyond the Maxwellian and Gaussian systems. As stated above, all of the desirable mathematical properties of the maximum-entropy closures assume that a maximum-entropy distribution function for the selected set of velocity moments always exists; this is not the case. Junk has shown that for any moment system based on moments, which correspond to super-quadratic polynomial weight functions, there are physically realizable combinations of the macroscopic moments for which a maximum-entropy distribution function is not valid and cannot be found [25–28]. Moreover, moment states describing local thermodynamic equilibrium always lie on the boundaries separating regions in moment space in which a maximum-entropy distribution function exists and is definable and those regions for which the maximum-entropy distribution cannot be found [26]. The latter correspond to regions in which $h(\boldsymbol{\alpha})$ is no longer differentiable, and therefore, the solution of the entropy minimization problem given by Eq. (32) does not exist. For this reason, there are near-equilibrium regions in moment space for which the higher order members of the Levermore maximum-entropy closures will become ill-posed or undefined. This is not a desirable feature for practical computations of non-equilibrium flows and it has prevented the wider application of the closures.

## 3 Gaussian moment closure

In spite of the evident limitations of the higher order members of the Levermore maximum-entropy hierarchy, the lowest order non-equilibrium solution, the Gaussian closure, is a physically realizable and hyperbolic moment closure. The potential of closures of this type for efficiently and accurately predicting both continuum and non-equilibrium flows is now demonstrated by considering the application of the Gaussian closure to a number of flow problems. In what follows, an extension of the Gaussian closure for diatomic gases is first described. This is followed by a discussion of a regularized form of the Gaussian closure that incorporates the effects of anisotropic heat flux. An arbitrary-Lagrangian–Eulerian (ALE) parallel finite-volume scheme with AMR and Riemann-solver-based numerical flux function is then described for solving the moment equations arising from these closures on multi-block meshes with embedded and possibly moving boundaries. Finally, the application of the closures to various continuum and non-equilibrium flow problems is examined.

### 3.1 Gaussian closure for monatomic and diatomic gases

For a monatomic gas, substitution of the distribution function of Eq. (34) into Maxwell's equation of change given in Eq. (5) leads to the following set of ten hyperbolic moment equations describing the transport of the quantities $\rho$, $\rho u_i$, and $P_{ij}$ [14,18,24]:

$$\frac{\partial}{\partial t}(\rho) + \frac{\partial}{\partial x_k}(\rho u_k) = 0, \tag{35}$$

$$\frac{\partial}{\partial t}(\rho u_i) + \frac{\partial}{\partial x_k}(\rho u_i u_k + P_{ik}) = 0, \tag{36}$$

$$\frac{\partial}{\partial t}\left(\rho u_i u_j + P_{ij}\right) + \frac{\partial}{\partial x_k}\left(\rho u_i u_j u_k + u_i P_{jk} + u_j P_{ik} + u_k P_{ij}\right) = -\frac{1}{\tau}\left(P_{ij} - \frac{\delta_{ij}}{3} P_{kk}\right), \tag{37}$$

where here the so-called relaxation-time or BGK approximation for the collision operator has been introduced in order to evaluate the collision terms [42] and $\tau$ is the relaxation or collision time.

The preceding equations are valid for a monatomic gas having no internal degrees of freedom or energy modes. A modification to the Gaussian closure is required to account for the additional internal energy that is associated with the extra internal degrees of freedom of diatomic molecules. Such an extension has been previously proposed by Hittinger [43] and was subsequently re-considered by McDonald and Groth [14]. This extension assumes that the Gaussian distribution function for a diatomic gas, $\mathcal{G}_{\mathrm{D}}$, takes the form

$$\mathcal{G}_{\mathrm{D}} = \frac{n^2 I}{(2\pi)^{5/2}(\det \boldsymbol{\Theta})^{1/2} p}\left(\frac{T}{T_{\mathrm{r}}}\right) \exp\left(-\frac{1}{2}\Theta_{ij}^{-1} c_i c_j\right) \exp\left(-\frac{1}{2} R_{\alpha\beta}\omega_\alpha \omega_\beta\right), \tag{38}$$

where $\omega$ is the angular velocity of the molecule, $I$ the moment of inertia of the molecule, $p$ the usual thermodynamic pressure, $T$ the temperature of the gas, $T_{\mathrm{r}}$ the rotational temperature, and $R_{\alpha\beta} = (nI/p)(T/T_{\mathrm{r}})\delta_{\alpha\beta}$. The extended closure then introduces an additional transport equation for internal rotational energy and makes use of a two-time-scale relaxation-time collision operator to model inter-particle collisions. The latter allows different relaxation times for the translational and rotational energy modes and approximate expressions are used to relate the relaxation times to the gas viscosity. The extension of the Gaussian closure for a diatomic gas results in the following moment equations:

$$\frac{\partial}{\partial t}(\rho) + \frac{\partial}{\partial x_k}(\rho u_k) = 0, \tag{39}$$

$$\frac{\partial}{\partial t}(\rho u_i) + \frac{\partial}{\partial x_k}(\rho u_i u_k + P_{ik}) = 0, \tag{40}$$

$$\begin{aligned}\frac{\partial}{\partial t}\left(\rho u_i u_j + P_{ij}\right) + \frac{\partial}{\partial x_k}\left(\rho u_i u_j u_k + u_i P_{jk} + u_j P_{ik} + u_k P_{ij}\right) \\ = -\frac{1}{\tau_{\mathrm{t}}}\left(P_{ij} - \frac{\delta_{ij}}{3} P_{kk}\right) - \frac{1}{15\tau_{\mathrm{r}}}\left(2P_{kk} - 3E_{\mathrm{r}}\right)\delta_{ij},\end{aligned} \tag{41}$$

$$\frac{\partial}{\partial t}(E_{\mathrm{r}}) + \frac{\partial}{\partial x_k}(u_k E_{\mathrm{r}}) = -\frac{1}{5\tau_{\mathrm{r}}}\left(3E_{\mathrm{r}} - P_{kk}\right), \tag{42}$$

where $E_{\mathrm{r}}$ is the energy of the rotational modes and $\tau_{\mathrm{t}}$ and $\tau_{\mathrm{r}}$ are the relaxation times associated with translational and rotational degrees of freedom, respectively.

### 3.2 Regularized Gaussian closure

For the Gaussian closure, the heat-flux tensor, $Q_{ijk}$, is zero by construction. This feature is one of the major shortfalls of the closure and makes it inappropriate for use in situations where the heat flux plays a significant role. McDonald and Groth [44] have recently considered a regularization of the Gaussian closure so as to re-introduce the effects of heat transfer. The regularization procedure is based on Chapman–Enskog expansion technique that can be applied to either the moment equations or the kinetic equation using the Gaussian distribution as the "base" distribution. When applied to the moment equations, the derivation follows the technique used by Struchtrup and Torrilhon in the regularization of the 13-moment equations [19]. The ellipsoidal-statistical collision operator proposed by Holway [40] is used in regularization analysis to represent inter-particle collision processes and ensure the correct values for fluid viscosity and thermal conductivity, and hence Prandtl number, $Pr$, in the continuum limit.

For the regularization of the Gaussian closure via a Chapman–Enskog perturbative expansion technique applied directly to the moment equations, it is first convenient to define the deviation of the fourth random-velocity moment from the corresponding fourth moment of the Gaussian distribution as

$$K_{ijkl} = m\left\langle c_i c_j c_k c_l \mathcal{F}\right\rangle - m\left\langle c_i c_j c_k c_l \mathcal{G}\right\rangle = m\left\langle c_i c_j c_k c_l \mathcal{F}\right\rangle - \frac{1}{\rho}\left[P_{ij}P_{kl} + P_{ik}P_{jl} + P_{il}P_{jk}\right]. \tag{43}$$

A smallness parameter, $\epsilon$, is then formally introduced and the scaled forms of generalized heat-flux tensor and deviatoric fourth-moment tensor in the general non-equilibrium case are expressed as perturbative expansions about the corresponding values predicted by the base Gaussian closure as follows:

$$Q_{ijk} = Q_{ijk}^{(\mathcal{G})} + \epsilon Q_{ijk}^{(1)} + \epsilon^2 Q_{ijk}^{(2)} + \epsilon^3 Q_{ijk}^{(3)} + \cdots , \tag{44}$$

and

$$K_{ijkl} = K_{ijkl}^{(\mathcal{G})} + \epsilon K_{ijkl}^{(1)} + \epsilon^2 K_{ijkl}^{(2)} + \epsilon^3 K_{ijkl}^{(3)} + \cdots . \tag{45}$$

Here, the superscript $(\mathcal{G})$ denotes the value predicted by the Gaussian distribution and the superscript $(n)$ denotes the $n$-th order correction to this value. A similar procedure is adopted for the regularization of the Gaussian closure via a Chapman–Enskog expansion applied to the phase-space distribution function. In this case, the scaled form of the perturbative expansion for the distribution is

$$\mathcal{F} = \mathcal{G}\left(g^{(\mathcal{G})} + \epsilon g^{(1)} + \epsilon^2 g^{(2)} + \epsilon^3 g^{(3)} + \cdots\right). \tag{46}$$

To zeroth-order, it is straightforward to show that $Q_{ijk}^{(\mathcal{G})} = 0$ and $g^{(\mathcal{G})} = 1$. If the Chapman–Enskog procedure is carried out to first-order, the following unscaled correction to the heat-flux tensor is obtained:

$$Q_{ijk}^{(1)} = \left\langle mc_i c_j c_k g^{(1)} \mathcal{G} \right\rangle = -\frac{\tau}{Pr}\left[P_{kl}\frac{\partial}{\partial x_l}\left(\frac{P_{ij}}{\rho}\right) + P_{jl}\frac{\partial}{\partial x_l}\left(\frac{P_{ik}}{\rho}\right) + P_{il}\frac{\partial}{\partial x_l}\left(\frac{P_{jk}}{\rho}\right)\right]. \tag{47}$$

In this anisotropic representation of thermal diffusion processes, the generalized heat-flux tensor is expressed in terms of the gradient of the pressure tensor and the coefficient of thermal conductivity is an anisotropic function of this same pressure tensor. The term would seem to represent a very natural anisotropic extension of Fourier's law and can be readily added to the Gaussian moment equations to incorporate the influences of non-equilibrium thermal transport.

It should be recognized that the addition of the expression for the generalized heat-flux tensor of Eq. (47) to the moment equations of the Gaussian closure spoils the hyperbolicity of the PDEs. Non-equilibrium thermal transport in this case is represented in terms of the gradient of other macroscopic quantities and this introduces an elliptic nature to the moment equations. Although the primary objective here is to explore hyperbolic descriptions of non-equilibrium gaseous flow behavior, this correction to the Gaussian closure following from the regularization procedure is useful in accessing the relative importance of the non-equilibrium thermal transport for the flows considered herein. It may also prove to be a rather inexpensive way of incorporating these effects into the Gaussian closure and arriving at a rather practical extended fluid-dynamics tool for representing anisotropic non-equilibrium transport phenomena.

### 3.3 Boundary conditions for solid walls

Appropriate solid-wall boundary conditions for the standard and regularized Gaussian closure have been developed by McDonald and Groth [14,44] using a Knudsen-layer analysis similar to that proposed by Grad [7]. The analysis allows for velocity slip directly and can account for temperature slip, in the case of the regularized closure, using standard temperature-slip boundary conditions developed in previous work [45]. These boundary conditions for the Gaussian closure at solid surfaces are used for obtaining all of the numerical solutions described herein. Please refer to the articles by McDonald and Groth [14,44] for further details. Additional analysis of solid-wall boundary conditions for the Gaussian closure is given in the recent article by Khieu et al. [46].

### 3.4 Godunov-type finite-volume scheme

A Godunov-type, ALE, parallel, upwind, finite-volume scheme with solution-directed block-based AMR and a treatment for embedded and possibly moving boundaries is proposed here for the numerical solution of the weak conservation form of the moment equations arising from the Gaussian-based closures described above (Gaussian closure for diatomic gases and the regularized Gaussian closure with heat transfer). Two-dimensional

flows are considered and the proposed solution algorithm is implemented on multi-block body-fitted quadrilateral meshes. An efficient and highly scalable parallel implementation is achieved via domain decomposition. The ALE treatment is used to deal with moving boundaries. Key aspects of the parallel AMR finite-volume scheme for embedded and moving boundaries are now described. For purely hyperbolic PDEs, the combination of Godunov-type finite-volume scheme with both the AMR and embedded mesh algorithms has been shown to produce both accurate and robust discretizations, even on highly irregular mesh having cut cells and/or large variations in the sizes of adjacent cells [16,17,22,23].

### *3.4.1 Spatial- and temporal-discretization procedures*

The moment equations of the extended form of the Gaussian closure for diatomic gases and the regularized Gaussian closure can be expressed in the following weak conservation form

$$\frac{\partial \mathbf{U}}{\partial t} + \vec{\nabla} \cdot \vec{\mathbf{F}} = \frac{\partial \mathbf{U}}{\partial t} + \vec{\nabla} \cdot \vec{\mathbf{F}}_{\mathrm{H}}(\mathbf{U}) + \vec{\nabla} \cdot \vec{\mathbf{F}}_{\mathrm{E}}(\mathbf{U}, \vec{\nabla}\mathbf{U}) = \mathbf{S} \tag{48}$$

where $\mathbf{U}$ is the vector of conserved moments, $\vec{\mathbf{F}}$ the moment flux dyad which can in general consist of a hyperbolic component, $\vec{\mathbf{F}}_{\mathrm{H}}(\mathbf{U})$, and an elliptic component, $\vec{\mathbf{F}}_{\mathrm{E}}(\mathbf{U}, \vec{\nabla}\mathbf{U})$, and $\mathbf{S}$ the vector of source terms representing the collisional processes. A Godunov-type upwind finite-volume spatial discretization procedure in conjunction with limited linear solution reconstruction and Riemann-solver based flux function are used to solve the preceding equations on two-dimensional multi-block domains composed of quadrilateral computational cells. The semi-discrete form of this finite-volume formulation applied to cell $(i, j)$ is given by

$$\frac{\mathrm{d}\mathbf{U}_{i,j}}{\mathrm{d}t} = -\frac{1}{A_{i,j}} \sum_{k} \left[ \left( \vec{\mathbf{F}} - \vec{w}\mathbf{U} \right) \cdot \vec{\mathbf{n}} \, \Delta\ell \right]_{i,j,k} - \left( \frac{\mathbf{U}}{A} \frac{\mathrm{d}A}{\mathrm{d}t} \right)_{i,j} + \mathbf{S}_{i,j}, \tag{49}$$

where $\mathbf{U}_{i,j}$ is the average solution in cell $(i, j)$, $A_{ij}$ the area of the cell, and $\vec{w}$, $\vec{\mathbf{n}}$, and $\Delta\ell$ the velocity of, unit normal to, and length of the $k$th cell face or edge, respectively. The term on the right-hand side of this equation containing the term $\mathrm{d}A/\mathrm{d}t$ corresponds to the time rate of change of the cell area. This term is approximated by the geometric conservation law, which states that the change in cell area is equal to the area swept by the moving surfaces [47]. The hyperbolic component of the numerical fluxes at the faces, $k$, for each cell are determined from the solution of a Riemann problem. Given left and right solution states, $\mathbf{U}_{\mathrm{l}}$ and $\mathbf{U}_{\mathrm{r}}$, at each cell interface, the numerical flux is given by

$$\vec{\mathbf{F}}_{\mathrm{H}} \cdot \vec{\mathbf{n}} = \mathcal{F}(\mathbf{U}_{\mathrm{l}}, \mathbf{U}_{\mathrm{r}}, \vec{\mathbf{n}}), \tag{50}$$

where the numerical flux $\mathcal{F}$ is evaluated by solving a Riemann problem in a direction defined by the normal to the face with initial data $\mathbf{U}_{\mathrm{l}}$ and $\mathbf{U}_{\mathrm{r}}$. The left and right solution states are determined via a least-squares piece-wise limited linear solution reconstruction procedure in conjunction with the slope limiter of Venkatakrishnan [48,49]. Roe's approximate Riemann solver [50] is used to solve the Riemann problem and evaluate the numerical flux. A suitable Roe linearization of the flux Jacobian of the Gaussian closure for monatomic gases has been determined by Brown et al. [11,12] and a similar linearization has been developed by Hittinger [43] for the diatomic case. Elliptic fluxes, $\vec{\mathbf{F}}_{\mathrm{E}}$, arising from anisotropic thermal-diffusion terms of the regularized Gaussian closure are evaluated using a diamond-path reconstruction technique [16,17,22,23]. Finally, the ordinary differential equations of Eq. (49) are integrated forward in time using a second-order-accurate point-implicit predictor–corrector time-marching scheme [14]. In the point-implicit treatment, the hyperbolic and elliptic fluxes are integrated explicitly and the collisional source terms are dealt with implicitly.

### *3.4.2 Adaptive mesh refinement and parallel implementation*

The solution of the moment equations by the finite-volume method outlined above provides area-averaged solution quantities within quadrilateral computational cells and these cells are embedded in structured body-fitted mesh blocks consisting of $N_{\mathrm{cells}} = N_i \times N_j$ cells, where $N_i$ and $N_j$ are even, but not necessarily equal, integers representing the number of cells in each logical coordinate direction of the block. Refer to Fig. 1. Mesh adaptation is accomplished by the dividing and coarsening of appropriate solution blocks. The refinement of the mesh is directed by physics-based refinement criteria as well as by other geometrical criteria related to the needs of accurately resolving embedded/moving boundaries. The AMR algorithm first flags blocks for either

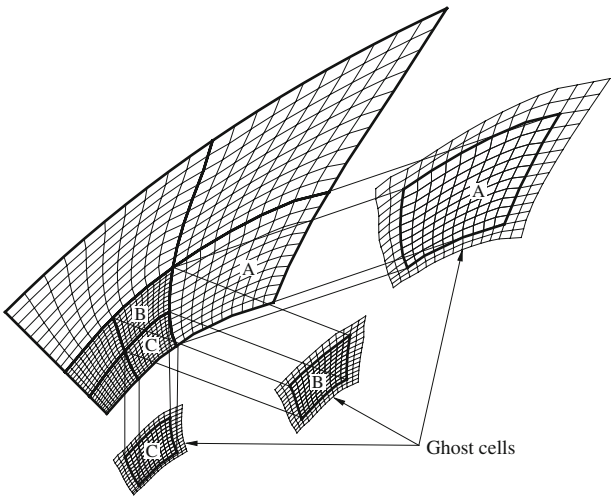


**Fig. 1** Multi-block body-fitted quadrilateral mesh of block-based AMR algorithm illustrating the layers of overlapping ghost cells used to facilitate inter-block communication

refinement or coarsening based on situation-dependent criteria and thresholds. Blocks flagged for refinement are subdivided into four "child" blocks, each of which has the same number of cells in each direction, as did the "parent" block, thus doubling the mesh resolution. If all four "child" blocks of one "parent" are later flagged for coarsening, the process can be reversed. Note, however, that no area of the mesh can be made coarser than it was originally and neighboring blocks are restricted to have a difference in refinement of at most one level. Standard restriction and prolongation operators are used to evaluate the solution on all blocks created by the coarsening and division processes, respectively.

A hierarchical quadtree data structure is use to keep track of the connectivity between solution blocks, an example of which can be seen in Fig. 2. Solution information is shared between adjacent blocks through the use of "ghost" or "halo" cells. Again refer back to Fig. 1. The flux conservation properties of the finite-volume scheme are preserved across block interfaces by using the interface fluxes computed on more refined blocks to correct the interface fluxes computed on coarser neighboring blocks. A primary advantage of the quadtree data structure is that it readily permits local mesh refinement. Local modifications to the multi-block mesh can be performed without re-gridding the entire mesh and re-calculating all solution block connectivity.

By design, the multi-block body-fitted AMR scheme is well suited to parallel implementation on distributed-memory multi-processor architectures via domain decomposition where solution blocks are simply distributed equally among the available processors, with more than one block permitted on each processor. Due to the similar nature of the solution blocks, an efficient decomposition can be readily achieved leading to high parallel efficiency and scalability. Parallel implementation of the block-based AMR scheme has been car-

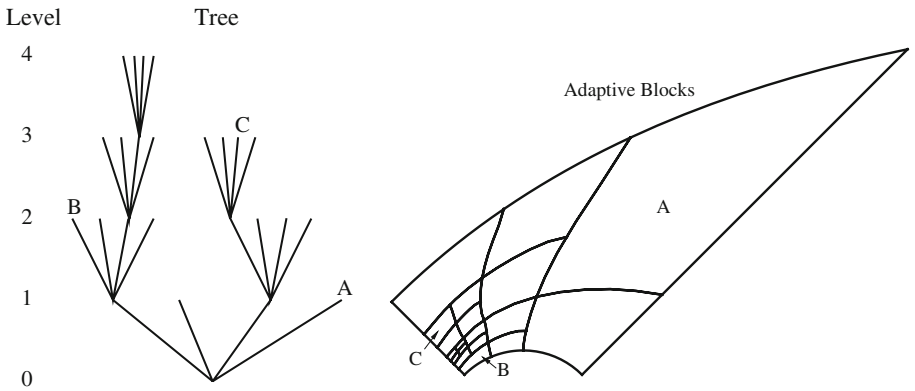


**Fig. 2** Schematic diagram illustrating quadtree data structure and the corresponding block-based refinement for a body-fitted mesh showing solution blocks at four different levels of refinement

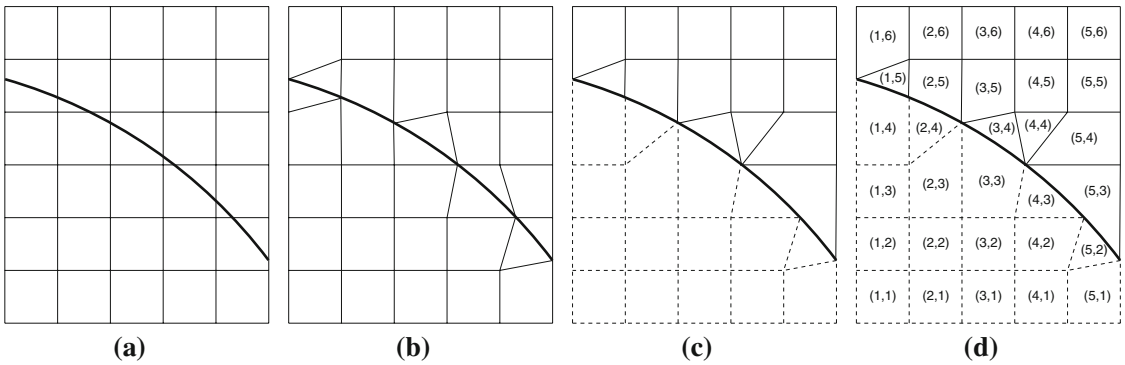


**Fig. 3** Illustration of steps taken during application of mesh adjustment algorithm: **a** initial mesh and embedded boundary (*thick line*), **b** result of primary adjustment, **c** result of secondary adjustment (*dashed lines* indicate inactive cells), and **d** preservation of $(i, j)$-indexing on final adjusted mesh

ried out using the MPI (message passing interface) library. Message passing of solution information between processors is largely limited to the asynchronous communication of ghost-cell solution values.

### *3.4.3 Embedded-mesh algorithm*

Implementation of the preceding finite-volume AMR scheme with the mesh-adjustment scheme proposed recently by Sachdev and Groth [16,17] has also been carried out. This mesh-adjustment scheme provides an automated treatment for fixed and moving, non-grid-aligned boundaries embedded in a body-fitted, multi-block mesh. By making only local alterations to the grid, this scheme enables the solution of unsteady flows involving moving boundaries or for steady flow problems involving stationary boundaries that are not necessarily aligned with the mesh, while preserving the structured nature of the blocks and avoiding the creation of small cut cells that are often generated by traditional cut-cell approaches. These features of the embedded mesh algorithm are illustrated in Fig. 3. The ratio of the smallest to largest neighbor cell areas produced by the proposed embedded boundary treatment has been found to be not less than about 0.2–0.25. In addition, the mesh adjustment algorithm is fully compatible with block-based AMR and parallel implementation via domain decomposition used in the finite-volume solution scheme described above.

The present implementation allows for moving embedded boundaries whose motion can be prescribed either explicitly or through a level-set method [51,52]. Boundary locations are computed at each time step and the mesh is readjusted. To avoid excessive tangling, the mesh is first returned to an unadjusted state and then readjusted. Cells near the boundary will, therefore, change shape and previously active cells may become inactive, or vice versa. The solution content in these cells is redistributed as described in the articles by Sachdev and Groth [16,17].

## 3.5 Numerical results

The application of the Gaussian closures to several canonical flow problems is now discussed. Results for both near equilibrium and general non-equilibrium flows are considered. Further examples of the application of the Gaussian closure to other similar flow problems are described by McDonald and Groth [14,44]. For all of the cases considered below, values for the mean free path, $\lambda$, used to define the Knudsen number were determined using the expression for hard sphere collisional processes given by Bird [3].

### *3.5.1 Subsonic laminar Couette flow*

The first case considered is planar subsonic Couette flow between two oppositely moving infinite plates [53]. Figure 4 shows both the predicted normalized flow velocity, $u/U$ and the normalized shear stress, $\tau_{xy}/\rho U\sqrt{2kT/\pi m}$, for the case of Couette flow between two plates moving in opposite directions at velocity $U = 30\,\text{m/s}$ with monatomic argon as the working gas at a temperature of $T = 293\,\text{K}$. It can be seen that the Gaussian closure correctly captures both the continuum and free-molecular solution behavior well. What

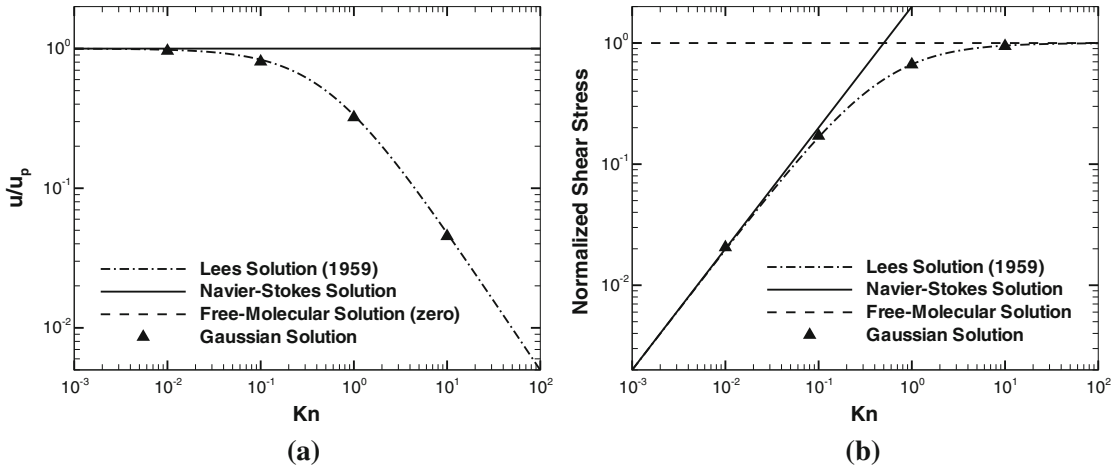


**Fig. 4** Predicted values of **a** the normalized flow velocity at the wall and **b** the normalized shear stress as a function of Knudsen number for planar subsonic Couette flow of argon between parallel diffusively reflecting walls; $U = 30\,\text{m/s}$, $T = 293\,\text{K}$. The numerical results for Gaussian closure are compared to analytic solutions based on continuum (Navier–Stokes) and free-molecular flow models, as well as an approximation due to Lees [53]

is more, it transitions from one to the other in excellent agreement with an the approximate analytical solution developed by Lees [53]. Although the good agreement in this case is more a validation of the solid-wall boundary conditions than the moment closure itself, it certainly demonstrates the promise of the moment closures.

### *3.5.2 Subsonic laminar flow past a circular cylinder*

The next case considered herein pertains to subsonic flow of air past a circular cylinder. The key influences of Knudsen number on the flow-field characteristics are first demonstrated by comparing the predicted solutions of the Gaussian closure for a diatomic gas for subsonic flow past a cylinder for two different Knudsen numbers but with a fixed speed ratio of $S = 0.027$. The speed ratio is the ratio of the bulk speed to the most probable random speed of a particle. Results for $Kn = 10^{-3}$ and $Kn = 1$ are given in Fig. 5. The figure shows that there are marked differences in the structure of the predicted continuum and non-equilibrium solutions. At a Knudsen number of $10^{-3}$, the velocity slip at the wall is negligible. The flow is clearly separated and there is a significant region of recirculation downstream of the cylinder. For a Knudsen number approaching unity, there is now appreciable velocity slip and the flow remains attached. There is also far greater symmetry between the upstream and downstream solutions of the Gaussian closure in this case.

There is a reasonably large quantity of data and theory results available in the literature for steady subsonic laminar flow past a circular cylinder. In particular, the coefficient of drag, $C_\text{d}$, is available for continuum, transitional, and free-molecular flow regimes. Figure 6 shows a comparison of experimental data collected by Coudeville and co-workers [54] with an approximate solution developed by Patterson [55], and solutions from the diatomic Gaussian closure for flow of air past a cylinder at two different speed ratios. The comparisons of Fig. 6 show that the Gaussian solutions are in very good agreement with the experimental results for the continuum regime and the transition regime. However, as the free-molecular regime is approached ($Kn > 1$), the numerical predictions of the drag coefficient provided by the Gaussian closure are somewhat high.

Before continuing, the capability of the mesh refinement scheme to resolve time-dependent flow situations with evolving regions of interest can be demonstrated through the prediction of von Kármán vortex shedding for the circular cylinder flow. Figure 7a shows density contours as predicted by the Gaussian moment closure for continuum flow of air with freestream Mach and Reynolds numbers of $M = 0.2$ and $Re = 100$, respectively. A section of the adaptive-mesh-refinement grid is shown in Fig. 7b. It can be seen that the AMR algorithm efficiently clusters cells in regions of high vorticity and effectively resolves the vortices being shed downstream of the cylinder. The computed Strouhal number for this case is 0.157, which agrees well with an experimental measurement of 0.164 by Williamson [56] and another computational result of 0.16 by Braza et al. [57].

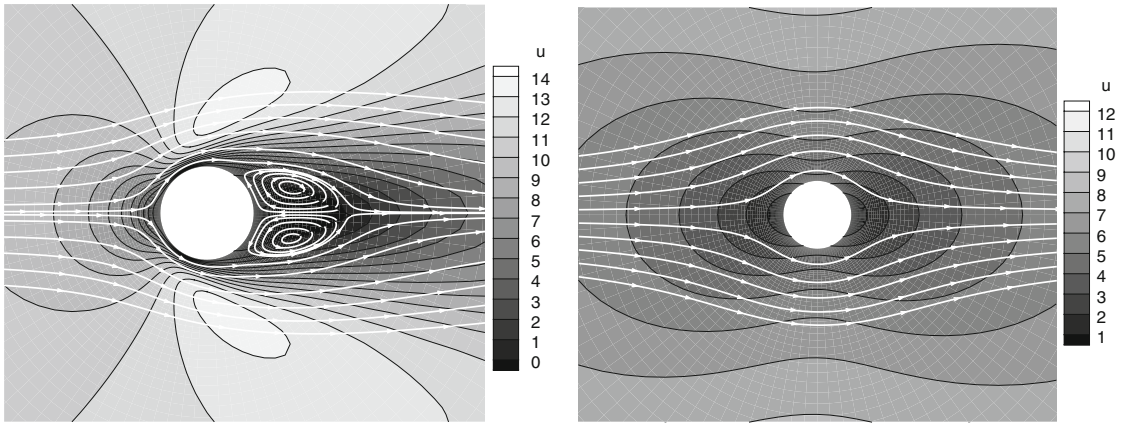


**Fig. 5** Predicted distributions of the $x$-direction velocity component for subsonic laminar flow of air past a circular cylinder at a speed ratio $S = 0.027$ obtained using the Gaussian closure for two different values of the Knudsen number: **a** $Kn = 10^{-3}$; and **b** $Kn = 1$

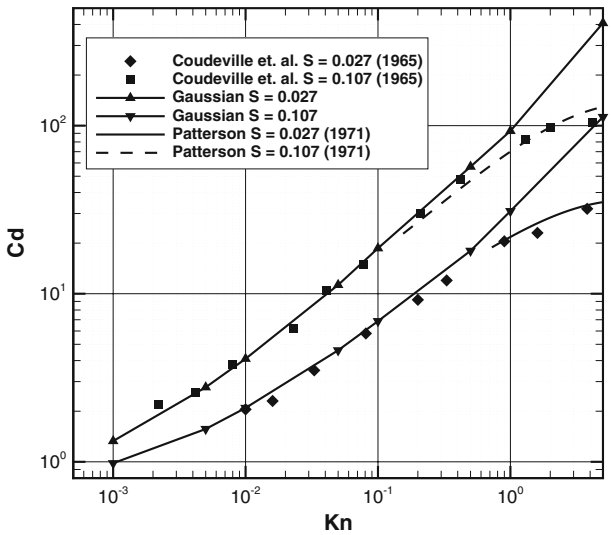


**Fig. 6** Coefficient of drag, $C_d$, for subsonic laminar flow of air past a circular cylinder at two different speed ratios, $S = 0.027$ and $S = 0.107$, respectively. The predicted drag coefficient obtained using the Gaussian closure are compared to the experimental results of Coudeville et al. [54] and the approximate solution due to Patterson [55]

### *3.5.3 Subsonic laminar flow past an embedded flat plate*

As discussed previously, the hyperbolic nature of the Gaussian moment equations makes them insensitive to grid irregularities. This can be demonstrated by considering subsonic boundary-layer flow of air past a flat plate which has been embedded in an aligned and unaligned mesh. For this situation, the freestream Mach and Reynolds numbers were $M = 0.2$ and $Re = 2000$, respectively, and the Knudsen number was $1.5 \times 10^{-4}$, which indicates that the flow is laminar and in the continuum regime. Two computational meshes are considered: one aligned with, or at 0° to, the plate and a second mesh at 30° to the plate. A section of the mesh with the plate at 30° is shown in Fig. 8a.

Numerical predictions of the friction coefficient, $C_f$, are shown in Fig. 8b. In the figure, comparisons are made to the classical, incompressible-flow, boundary-layer results of Blasius [58]. It can be seen that there is good agreement between the computed results using the Gaussian closure and the Blasius solution. Furthermore, there are no oscillations present in the predicted skin friction coefficients, even when the flat plate intersects the grid at an angle. Such oscillations are often generated when solving PDEs on irregular meshes

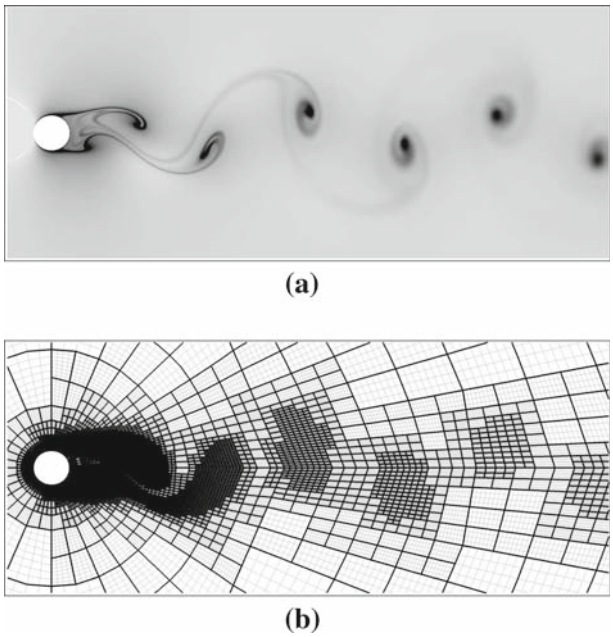


**Fig. 7** Prediction of unsteady vortex shedding for laminar subsonic continuum flow of air past a circular cylinder with freestream Mach and Reynolds numbers of $M = 0.2$ and $Re = 100$, respectively showing: **a** the predicted distribution of flow density obtained using the Gaussian closure; and **b** the AMR grid used in performing the unsteady computations

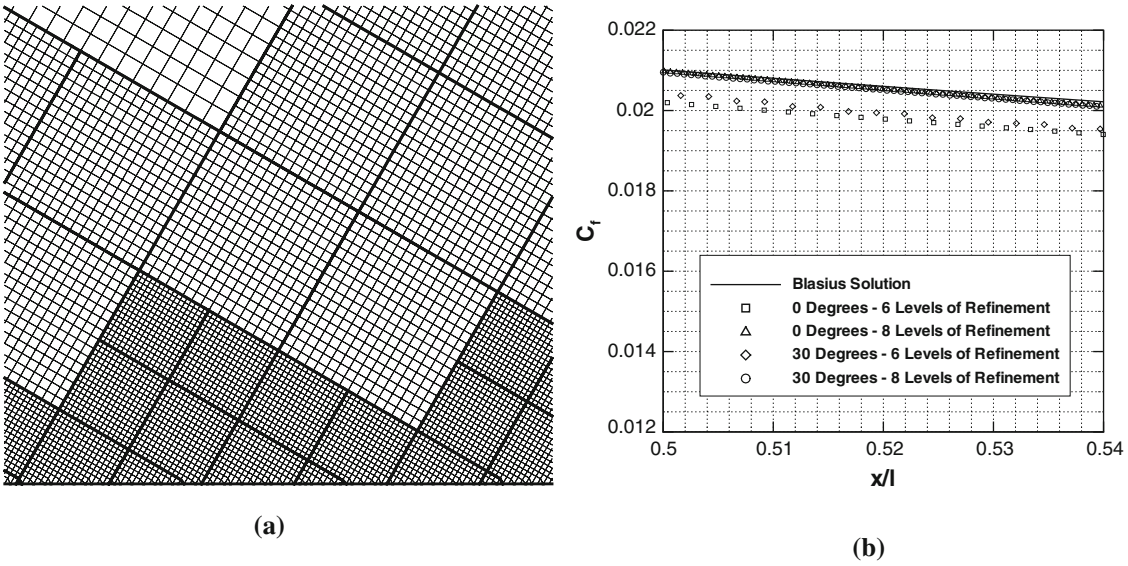


**Fig. 8** Predicted subsonic laminar flow of air past an embedded flat plate showing **a** a portion of the 65024-cell non-aligned mesh with flat plate embedded at 30° to the frame of the mesh and **b** predicted coefficient of friction, $C_f$, calculated using the Gaussian closure for a Cartesian grid aligned with an embedded flat plate at 0° compared to the predicted drag coefficient obtained for a non-aligned plate at 30° to the grid. The predicted coefficients of friction are also compared to the Blasius solution

such as this, with solution fluxes having elliptic components, as is the case for the Navier–Stokes equations [22,23].

### *3.5.4 Subsonic laminar flow past an embedded circular cylinder*

As a further demonstration of the insensitivity of the Gaussian closure to grid irregularities and in order to demonstrate that the embedded-boundary treatment can recover the drag results for the circular cylinder described

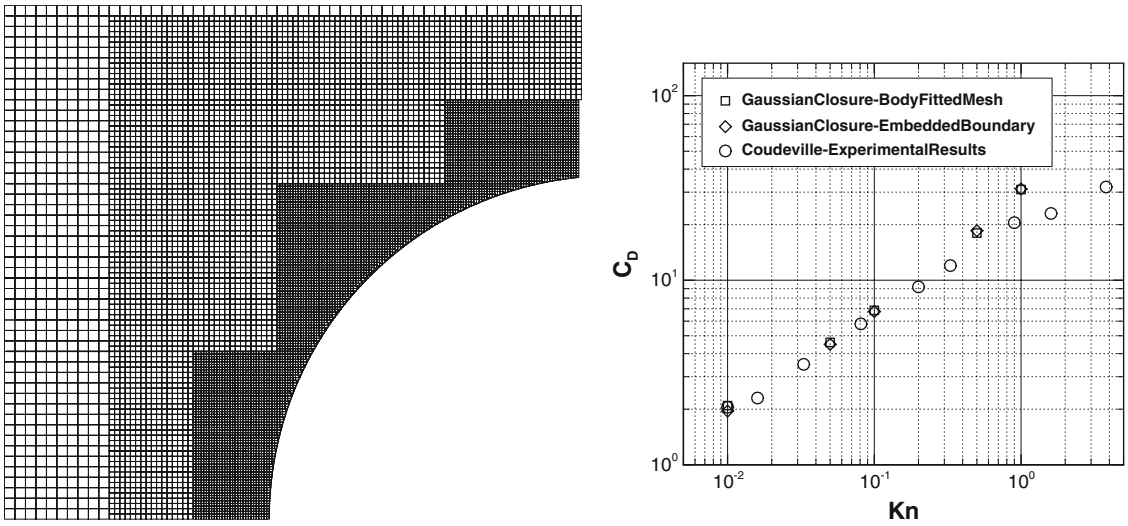


**Fig. 9** Predicted subsonic laminar flow of air past an embedded circular cylinder showing **a** a portion of the computational grid and the embedded circular cylinder and **b** the predicted coefficients of drag, $C_d$, computed using the Gaussian closure with a body-fitted mesh and the Cartesian mesh with the embedded boundary treatment, for a speed ratio of $S = 0.107$. The predicted drag coefficients are also compared to the experimental results of Coudeville et al. [54]

above with virtually equal accuracy to those obtained with a body-fitted mesh, values for the coefficient of drag were re-computed using the Gaussian closure and embedded mesh approach for a range of Knudsen numbers with a speed ratio of 0.107. The computed coefficients of drag are shown in Fig. 9b. A section of the embedded mesh with the embedded circular boundary is shown in Fig. 9a. It can be seen that agreement between the experimental results and the values predicted by the Gaussian closure are equally good when the embedded boundary treatment is used.

### *3.5.5 Subsonic laminar flow past a NACA*0012 *micro-airfoil*

As a final example and to illustrate the importance of heat transfer in many transition-regime flow problems, transonic steady flow of air around a NACA0012 micro-airfoil at zero angle of attack is considered. For the case of interest, the freestream Mach and Reynolds numbers are $M = 0.8$ and $Re = 73$, respectively, and the Knudsen number is $Kn = 0.017$ based on the chord length. Numerical predictions for this flow were obtained using both the standard and regularized Gaussian moment equations, with extensions for a diatomic gas, and are given in Fig. 10a and b, respectively. Numerical predictions of the distribution of the flow density are shown in the figures. For comparison, results obtained using a DSMC scheme by Sun and Boyd [6] and corresponding experimental results based on the measurements of Allegre, Raffin and Lengrand [59] are also reproduced here in Fig. 10c and d.

It is evident from the comparisons of Fig. 10a–d that the predictions obtained using the standard Gaussian closure (i.e., the moment closure without heat transfer) agree surprisingly well with both the DSMC and experiment results in the vicinity of the leading edge of the airfoil. In fact, the 10-moment model provides a better estimate of the stagnation-point density than the DSMC method, which tends to strongly overestimate this value. The disagreement with DSMC results and experimental measurements in the stagnation region illustrates the imperfections, uncertainties, and challenges with predicting micro-scale non-equilibrium flows, even with particle-based methods.

In spite of the good predictive capabilities of the Gaussian model for the leading edge region of the airfoil, the moment closure results in predicted flow densities that seem to be very much under-predicted along the length of the airfoil towards the trailing edge. A similar finding was reported in the previous work of Suzuki and van Leer [60]. While it may be argued that some of this disagreement between the Gaussian closure and DSMC and experimental data may be attributed to the application of boundary conditions, the inclusion of thermal diffusion via the regularized Gaussian closure provides greatly improved agreement between the moment closure results and those of both DSMC and experiment, particularly towards the trailing edge of

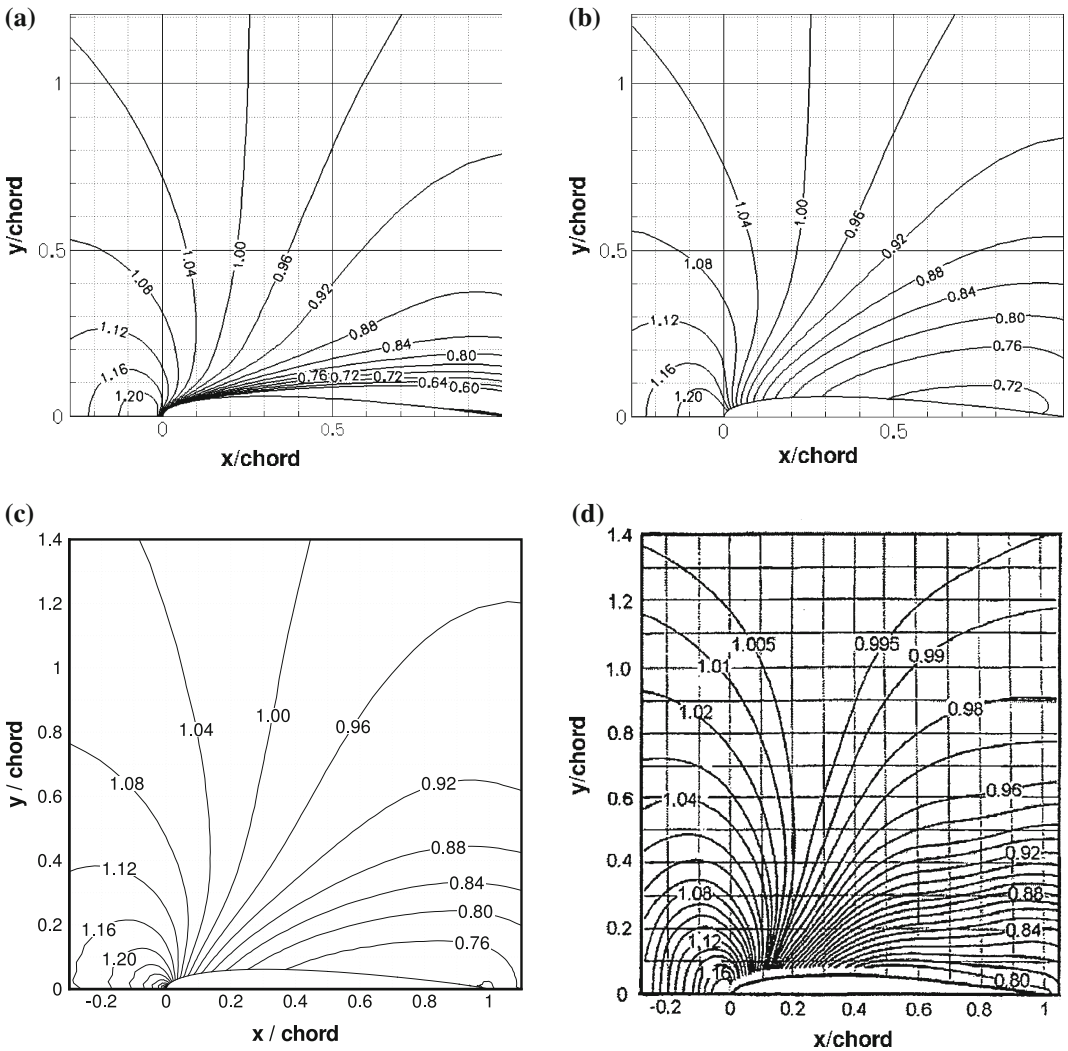


**Fig. 10** Comparison of the distribution of the normalized flow-field density for transonic flow of air around a NACA0012 micro-airfoil with freestream Mach, Reynolds, and Knudsen numbers of $M = 0.8$ $Re = 73$, and $Kn = 0.017$, respectively: **a** predictions of the standard Gaussian moment closure; **b** predictions of the the regularized Gaussian moment closure; **c** predictions of the DSMC method of Sun and Boyd [6]; and **d** experimental data of Allegre, Raffin, and Lengrand [59]

the airfoil. In general, the overall agreement between the regularized Gaussian and DSMC and experimental results are very good and this strongly indicates the importance of non-equilibrium heat transfer for this class of flow problem. The comparisons would also suggest that a physically realizable and hyperbolic moment closure, which properly accounts for non-equilibrium thermal transport, has the potential to perform well for problems of this type.

## 4 Physically-realizable and hyperbolic moment closures

As discussed in Sect. 2.5 above, for any member of the Levermore maximum-entropy hierarchy of order higher than the Gaussian closure, Junk has shown that there exist physically realizable moments for which a maximum-entropy distribution function cannot be found [25,26]. This issue is related to the inability to satisfy simultaneously all of the restrictive conditions on the closure coefficients, $\boldsymbol{\alpha}$, which ensure that the polynomial $\mathcal{P}^{(N)}(\vec{v}) = \boldsymbol{\alpha}^{\mathrm{T}}\mathbf{V}^{(N)}$ decreases toward negative infinity in all directions as $|\vec{v}|$ becomes large. More devastating still, for these higher-order moment closures, equilibrium solutions lie on the boundary in moment space separating regions in which the entropy maximization problem can be solved and regions in which a solution is

not possible [26], leaving little hope that numerical solutions to these moment closures can be computed for any practical situations.

### 4.1 Modified distribution function

One possible technique to avoid issues with non-realizability of maximum-entropy closures is to modify slightly the assumed form for the distribution function. This can be accomplished by adding an additional term, $\sigma$, to the exponential of Eq. (14) to yield

$$\mathcal{F}^{(N)} = \exp\left(\mathcal{P}^{(N)}(\vec{v}) + \sigma\right) = \exp\left(\boldsymbol{\alpha}^{\mathrm{T}}\mathbf{V}^{(N)} + \sigma\right) = \exp\left(\boldsymbol{\alpha}^{\mathrm{T}}\mathbf{V}^{(N)}\right) f_{\mathrm{w}}, \tag{51}$$

where $f_{\mathrm{w}} = e^{\sigma}$. This type of modification to the maximum-entropy moment distribution seems to have been first proposed by Au [61] and then later re-considered by Junk (unpublished work). The modification is equivalent to multiplying the distribution function by a factor $f_{\mathrm{w}}$. This factor can be viewed as a "window" function that attenuates the distribution at high velocities. In general, $\sigma$ is a velocity-dependent term that must be chosen such that it approaches negative infinity more quickly than the polynomial, $\boldsymbol{\alpha}^{T}\mathbf{V}^{(N)}$, can approach positive infinity as $|\vec{v}|$ becomes large. This will allow the closure to remain valid for all physically realizable sets of velocity moments.

In the case that $\sigma$ is not a function of the closure coefficients, proof of hyperbolicity as described above remains valid and the hyperbolic properties of the moment closure are retained. A simple example where this is true is to take $\sigma = -b|\vec{v}|^{n}$ where $b$ is a positive real value and $n$ is an even integer larger than the highest power of the velocity weights in $\mathbf{V}^{(N)}$. In this case, $\partial\sigma/\boldsymbol{\alpha} = 0$ and the proof of hyperbolicity remains unaltered. Unfortunately, the closure is no-longer Galilean invariant for this choice of $\sigma$. Taking $\sigma = -b|\vec{c}|^{n}$ leads to a Galilean-invariant closure; however, in this case, $\partial\sigma/\boldsymbol{\alpha} \neq 0$ and hyperbolicity of the closure is not assured. This is because it is no longer possible to ensure that $h_{\alpha\alpha}$ is symmetric positive definite.

In practice, it would seem prudent to define $\sigma$ to be a function of the local solution so as to ensure Galilean invariance of the closure. Moreover, it would also seem desirable to have the coefficient $\sigma$ be dependent on the solution so as to match the standard deviation of the unmodified distribution in some way and thereby result in a more effective windowing function. In the current work, the modification to the maximum-entropy distribution is chosen to have the form

$$\sigma = -b\left(\frac{\rho}{p}\right)^{\frac{L+2}{2}} |\vec{c}|^{L+2}, \tag{52}$$

where $L$ is the highest exponent of the velocity weights used in the moment closure and $b$ is some specified positive number. This form for $\sigma$ clearly makes strict proof of hyperbolicity elusive; however, it can be shown through numerical experiments that the resulting moment equations are well behaved and remain hyperbolic for a wide range of flow conditions.

One cause for concern with this proposed approach may be its treatment of equilibrium conditions as the modified distribution function no longer contains the Maxwellian. Nevertheless, under equilibrium conditions, the moments of the modified distribution function used in the closure are in full agreement with those of the Maxwellian up to one order higher than the order of the closure provided that the velocity weights of the Levermore hierarchy are used. In addition, all odd-order random velocity moments of the modified assumed-form for the distribution function vanish and are equal to those of the Maxwellian under equilibrium conditions.

It should be noted that with the introduction of the window function no longer requires the strict use of the velocity weights, $\mathbf{V}^{(N)}$ or $\mathbf{C}^{(N)}$, proposed in the Levermore hierarchy as the window function can be used to ensure that the distribution approximate function remains finite. Other choices are, therefore, possible for the velocity moments of the closure while still remaining both realizable and hyperbolic (Junk, M., unpublished work). Additionally, Schneider [27,28] has proposed an alternate approach to dealing with the realizability of maximum-entropy closures. He proposes appropriately relaxing some of the equality constraints on the moments in the entropy minimization procedure when defining the maximum-entropy distribution. This leads to a maximum-entropy solution; however, it is one that does not satisfy the full set of predicted moments (only those that can be satisfied and represented by the maximum-entropy distribution). Hauck et al. [28] have subsequently carried out a mathematical analysis of this alternate approach to modifying maximum-entropy closures and have developed a geometrical description of the regions in realizable moment space where the standard maximum-entropy closures fail or breakdown.

### 4.2 Application to a one-dimensional gas

In order to explore the behavior of the proposed modification to the maximum-entropy hierarchy of Levermore, the moment closures are applied to the solution of non-equilibrium flows for a one-dimensional gas. In the case of a simple one-dimensional gas, particles are free to move only on a line and the kinetic equation can be written as

$$\frac{\partial \mathcal{F}}{\partial t} + v\frac{\partial \mathcal{F}}{\partial x} = -\frac{1}{\tau}\left(\mathcal{F} - \mathcal{M}\right), \tag{53}$$

where a BGK relaxation time approximation has been introduced to model collisional processes and the equilibrium distribution function or Maxwellian, $\mathcal{M}$, is given by

$$\mathcal{M} = \frac{\rho}{\sqrt{2\pi}ma_\circ}\exp\left(-\frac{(v-u)^2}{2a_\circ^2}\right) = \frac{\rho}{\sqrt{2\pi}ma_\circ}\exp\left(-\frac{c^2}{2a_\circ^2}\right), \tag{54}$$

with $a_\circ = \sqrt{p/\rho}$. Macroscopic quantities or velocity moments of interest in this case include the density, $\rho$, flow velocity, $u$, pressure, $p$, sound speed, $a$, heat flux, $q$, and fourth and fifth moments, $r$ and $s$, respectively:

$$\rho = m\left\langle \mathcal{F}\right\rangle, \quad u = \frac{m}{\rho}\left\langle v\mathcal{F}\right\rangle, \quad m\left\langle c\mathcal{F}\right\rangle = 0, \tag{55}$$

$$\rho u^2 + p = m\left\langle v^2\mathcal{F}\right\rangle, \quad p = m\left\langle c^2\mathcal{F}\right\rangle, \quad a^2 = 3\frac{p}{\rho} = 3a_\circ^2, \tag{56}$$

$$q = m\left\langle c^3\mathcal{F}\right\rangle, \quad m\left\langle c^4\mathcal{F}\right\rangle = r = 3\frac{p^2}{\rho} + \kappa, \quad m\left\langle c^5\mathcal{F}\right\rangle = s. \tag{57}$$

For the one-dimensional gas, there exists a member of the Levermore hierarchy whenever the highest order velocity moment is of even order. Members of this maximum-entropy hierarchy include the 3- and 5-moment closures with

$$N = 3, \quad \mathbf{C}^{(3)} = [1, c, c^2]^{\mathrm{T}}, \quad \mathbf{M}^{(3)} = [\rho, \rho u, p]^{\mathrm{T}}, \tag{58}$$

$$N = 5, \quad \mathbf{C}^{(5)} = [1, c, c^2, c^3, c^4]^{\mathrm{T}}, \quad \mathbf{M}^{(5)} = [\rho, \rho u, q, r]^{\mathrm{T}}, \tag{59}$$

and the assumed form of the distribution functions, $\mathcal{F}^{(N)} = \exp(\mathcal{P}^{(N)}(v))$, are given by

$$\mathcal{F}^{(3)} = e^{\alpha_0+\alpha_1 v+\alpha_2 v^2}, \quad \mathcal{F}^{(5)} = e^{\alpha_0+\alpha_1 v+\alpha_2 v^2+\alpha_3 v^3+\alpha_4 v^4}. \tag{60}$$

### 4.3 5-Moment closure

As a first step in the examination of the proposed closures, the 5-moment closure is considered. The PDEs describing the transport of the five lowest order macroscopic moments in this case are given by

$$\tfrac{\partial \rho}{\partial t} + \tfrac{\partial}{\partial x}\left(\rho u\right) = 0, \tag{61}$$

$$\tfrac{\partial}{\partial t}\left(\rho u\right) + \tfrac{\partial}{\partial x}\left(\rho u^2 + p\right) = 0, \tag{62}$$

$$\tfrac{\partial}{\partial t}\left(\rho u^2 + p\right) + \tfrac{\partial}{\partial x}\left(\rho u^3 + 3up + q\right) = 0, \tag{63}$$

$$\tfrac{\partial}{\partial t}\left(\rho u^3 + 3up + q\right) + \tfrac{\partial}{\partial x}\left(\rho u^4 + 6u^2 p + 4uq + r\right) = -\tfrac{q}{\tau}, \tag{64}$$

$$\tfrac{\partial}{\partial t}\left(\rho u^4 + 6u^2 p + 4uq + r\right) + \tfrac{\partial}{\partial x}\left(\rho u^5 + 10u^3 p + 10u^2 q + 5ur + s\right) = -\tfrac{4uq+r-3\frac{p^2}{\rho}}{\tau}. \tag{65}$$

Here, $s = m\left\langle c^5\mathcal{F}^{(5)}\right\rangle$ is the fifth-order random-velocity moment It is this fifth-order moment which must be determined through the integration of the assumed form of the distribution function to close the system. For the 5-moment closure, the modified form for the distribution function is given by

$$\mathcal{F}^{(5)} = e^{\alpha_0+\alpha_1 c+\alpha_2 c^2+\alpha_3 c^3+\alpha_4 c^4-b(\rho/p)^3 c^6} = e^{\alpha_0+\alpha_1 c+\alpha_2 c^2+\alpha_3 c^3+\alpha_4 c^4}e^{-b(\rho/p)^3 c^6}, \tag{66}$$

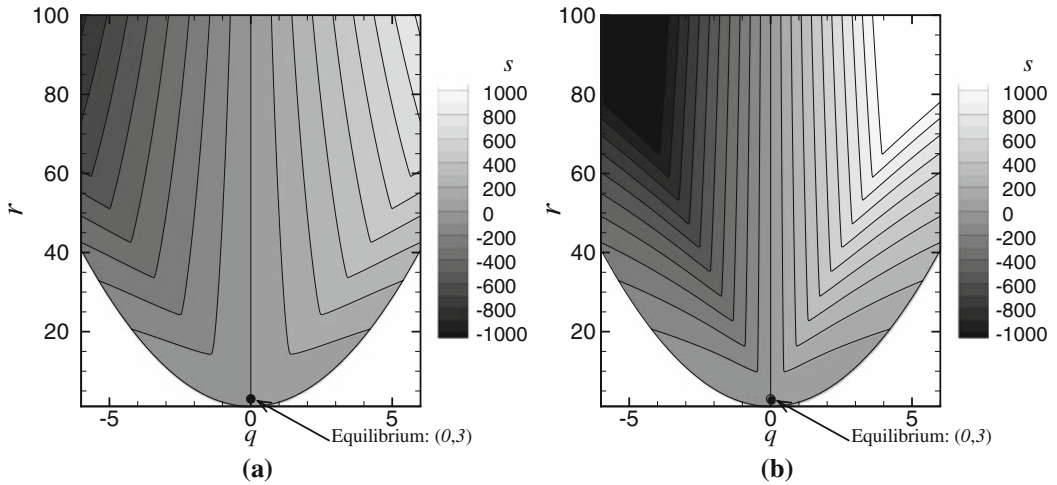


**Fig. 11** Predicted fifth-order random-velocity moment, $s$, as a function of $q$ and $r$ for the 5-moment one-dimensional realizable moment closure with **a** $b = 10^{-4}$; and **b** $b = 10^{-5}$

where $f_{\mathrm{w}} = e^{-b(\rho/p)^3 c^6}$ is the window function. The parameter $b$ can be adjusted to control the range of realizability for the closure. For $b = 0$, the maximum-entropy closure is recovered.

Without loss of generality, the distribution function of the 5-moment closure can be normalized such that it describes a gas with a density of one, a bulk velocity of zero and a pressure of one [25]. The relationship of the fifth-order moment $s$ can then be examined as a function of the normalized heat flux $q$ and fourth-order moment $r$. It can be shown [25] that, for this normalized situation, the complete solution phase space of the 5-moment closure is fully represented by the two-dimensional $(q, r)$ space and $r > 1 + q^2$ must be satisfied for the specified moments to be physically realizable in the sense described earlier in the paper. Figure 11 shows the numerical computation of $s$ as predicted by the new closure for a wide range of physically realizable situations for $b = 10^{-4}$ and $b = 10^{-5}$. For these two values of $b$, the modified realizable distribution function fully spans the region in $(q, r)$ space of all realizable moments and values for $s$ are computable. In fact, the proposed closure is realizable for all positive non-zero values of $b$. It is interesting to note that $s$ does not appear to be a smooth function of $q$ and $r$ as indicated by the sharp changes in the contour lines.

From Fig. 11, it is evident that the modification to the maximum-entropy distribution function has resulted in a moment closure, which covers the whole realizable moment space; however, formal proof of global hyperbolicity is not possible in this case. Hyperbolicity of the proposed closure is instead investigated numerically. The flux Jacobians are computed numerically using a second-order accurate centered finite-difference technique. Eigenvalues of the Jacobians, $\Lambda$, are then computed numerically. The system of moment equations is deemed hyperbolic whenever the eigenvalues are real. Figure 12 shows the largest imaginary part of the computed eigenvalues as a function of $q$ and $r$ for the normalized distribution function, again for the cases where $b = 10^{-4}$ and $b = 10^{-5}$. The computed eigenvalues do not remain real, and hence, the system is not globally hyperbolic. Fortunately, as $b$ decreases, the region of hyperbolicity expands greatly. It should be obvious that for $b = 0$ the closure will be hyperbolic but not realizable and as $b$ is increased the closure is now realizable but the region of hyperbolicity is reduced and does not span the full range of realizable moments. This points to a trade-off in the selection of the realizability parameter $b$: it must be non-zero and large enough so that all moments are numerically integrable ("numerically realizable") but sufficiently small so that the closure remains hyperbolic for the non-equilibrium flow conditions of interest.

In order to gain a feel for the degree of non-equilibrium behavior, which is contained in the hyperbolic region, the orbits of moments describing the structure of shock waves with shock Mach numbers of 2, 4, and 8 as predicted by a high-resolution numerical solution of the BGK kinetic equation (Eq. 2) are shown in both Figs. 12a and b. The orbit corresponding to a shock with an upstream Mach number of 2 is quite small as compared to that of the stronger shocks. The size of the orbits in this non-dimensional $(q, r)$ phase space, $\Gamma$, is estimated to scale with the shock Mach number, $M$, with a scaling something like $\Gamma \propto (M-1)^{1.83}$. It can be observed that, if $b$ is taken to be $10^{-5}$, even for the relatively high shock-Mach-number case, the moment

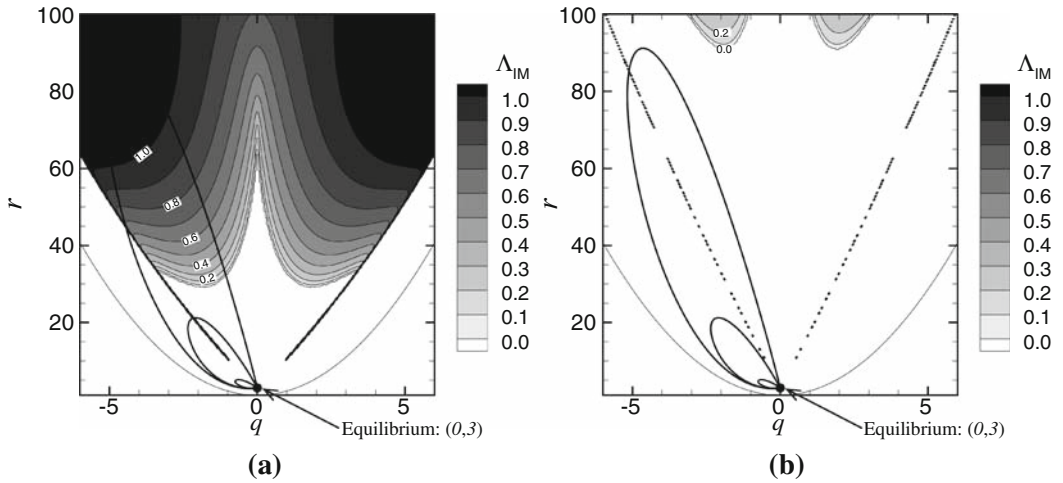


**Fig. 12** Largest imaginary part of the numerically determined eigenvalues of flux Jacobian for the modified, realizable, 5-moment moment closure with **a** $b = 10^{-4}$; and **b** $b = 10^{-5}$. The orbits of velocity moments corresponding the transition and internal structure for stationary shock wave solutions with shock Mach numbers of $M = 2$, $M = 4$, and $M = 8$ are also shown with the larger orbits corresponding to the higher shock Mach numbers

closure remains in the hyperbolic region. The appearance of complex eigenvalues along the line across which $s$ seems to be a non-smooth function of $q$ and $r$ is most likely due to the unsuitability of finite differences across this line. The hyperbolic nature of the closure and its moment equations is difficult to evaluate on this line.

### 4.4 Godunov-type finite-volume scheme

As a preliminary investigation of the predictive capability offered by the proposed higher order realizable hyperbolic moment equations, a numerical solution procedure has also been constructed for the one-dimensional moment system described above. The moment equations are solved using a Godunov-type finite-volume scheme. The HLL [62] approximate Riemann solver is used to evaluate inter-cellular fluxes, for which estimates for the maximum and minimum wave speeds are based on the numerical evaluation of the eigenvalues of an approximate flux Jacobian for the moment closure. Higher order accuracy is achieved through piecewise limited linear reconstruction and a point-implicit predictor–corrector time-marching scheme is again used to advance the solution [14].

For the 5-moment closure, there is no explicit conversion from conserved moments, $\mathbf{U} = \mathbf{M}^{(N)}$, to the closure coefficients, $\boldsymbol{\alpha}$. The evaluation of the highest-order flux requires that all of the coefficients be known at each time step. These coefficients can be determined by finding the solution to Eq. (31) with the modified distribution function used to define a modified density potential. This leads to a minimization problem given by

$$\mathcal{S}(\mathbf{M}^{(N)}) = -\min_{\boldsymbol{\alpha}} \left[ \left\langle \exp\left( \boldsymbol{\alpha}^{\mathrm{T}} \mathbf{V}^{(N)} + \sigma \right) \right\rangle - \boldsymbol{\alpha}^{\mathrm{T}} \mathbf{M}^{(N)} \right]. \tag{67}$$

Although the resulting solution, $\mathcal{S}$, from the minimization of the functional given in Eq. (67) above is no longer the mathematical entropy and the corresponding distribution function is not the maximum-entropy distribution, the minimization process still defines the relationship between the predicted moments and closure coefficients. As this function can be shown to be convex, the minimization problem can be solved using an approximate Newton's method. In some cases, it is possible for the computed update from Newton's method to move the vector $\boldsymbol{\alpha}$ to a location where numerical integration of the moments is not possible. When this happens, a back-tracking technique is used to step back into a computable region of moment space.

This technique for synchronization of $\boldsymbol{\alpha}$ and $\mathbf{U}$ involves many numerical integrations of the velocity distribution function and is quite computationally expensive compared to the other elements of the one-dimensional

flow solver. A technique to reduce the number of re-synchronizations required is, therefore, very desirable. One possibility is to again make use of the Hessian of the density potential, $\partial^2 h/\partial \boldsymbol{\alpha}^2 = \partial \boldsymbol{U}/\partial \boldsymbol{\alpha}$, to update the closure coefficients after each time step by exploiting the relationship

$$\Delta \boldsymbol{\alpha} = \left(\frac{\partial \mathbf{U}}{\partial \boldsymbol{\alpha}}\right)^{-1} \Delta \mathbf{U}. \tag{68}$$

If this update of the coefficients is sufficiently accurate, re-synchronization of $\boldsymbol{\alpha}$ in terms of $\mathbf{U}$ may not be required, thus greatly reducing the cost of the scheme. However, determining the effectiveness of this simplified update and deciding when a full re-synchronization is required can be somewhat difficult. One possibility is to apply the simple update above and integrate one velocity moment and compare it to the target value. A large deviation in the two values can be used as a trigger for a full re-synchronization.

### 4.5 Numerical results for stationary shocks

Predictions of the structure of stationary shocks for the one-dimensional gas obtained by solving the 5-moment version of the physically realizable moment equations are now considered. The numerical results are shown in Fig. 13 and compared with numerical solutions to the equivalent "Navier–Stokes" equations for a range of shock Mach numbers. High-resolution numerical solutions of the one-dimensional BGK kinetic equation for this one-dimensional gas are also depicted for comparison. The discrete-velocity method of Mieussens [4] is used to obtain the numerical solution of the one-dimensional kinetic equation. It can be seen that even at high Mach numbers, where the Navier–Stokes equations do a poor job of predicting shock structure, the hyperbolic 5-moment system agrees surprisingly well with the numerical solutions of the full kinetic equation.

### 4.6 Numerical results for the Riemann problem

In order to explore further the behavior of the modified 5-moment closure across a range of Knudsen numbers, a Riemann initial value problem is considered. The case of interest consists of a two-state initial condition with a pressure ratio of 2.5 and a density ratio of 2. Three different situations were examined corresponding to Knudsen numbers of $2.3 \times 10^{-5}$, $2.3 \times 10^{-2}$, and 23, thus spanning the continuum, transition, and free-molecular flow regimes. The resulting solutions are shown in Fig. 14. Here the 5-moment system is compared to the 3-moment closure (which is equivalent to the Euler equations for a one-dimensional gas), high-resolution numerical solutions of the BGK kinetic equation, and numerical solution of the equivalent "Navier–Stokes" equations. Again, the discrete-velocity method of Mieussens [4] is used to obtain the kinetic solutions.

It can be seen in Fig. 14a that, in the continuum regime, all three non-equilibrium solutions treatments are in close agreement with the equivalent "Euler" equations for this one-dimensional gas. On this scale of interest, the regions of the flow, which are not in local thermodynamic equilibrium, are much smaller than the domain of interest and are generally not resolved.

Figure 14b depicts the numerical results for the transition regime, lying somewhere between continuum and free-molecular results. In this regime, the 3-moment model, which can only correctly account for flows in thermodynamic equilibrium, gives an identical solution, although on a different scale, to that found for the continuum regime. The non-equilibrium solutions of the 5-moment model, Navier–Stokes equations, and BGK equation on this scale are all still quite similar to each other in this case, but are now quite distinct from the equilibrium or equivalent "Euler" result. For the non-equilibrium solutions, the wave structures that appear as discrete near discontinuities in the continuum situation are still identifiable but are now quite diffuse and approach one another such that they interact, yielding a solution with a smooth transition between the two constant initial states at either end of the solution domain.

The free-molecular results for the Riemann initial value problem are given in Fig. 14c. For this case, the 3-moment model again yields results that are the same as those for the continuum flow solution. For the modified 5-moment model, due to infrequent inter-particle collisions, the terms associated with the collision operator have now become so insignificant that the moment closure essentially behaves as a purely hyperbolic system without relaxation. It yields a solution with five separate or distinct waves separated by essentially constant solution states. This non-equilibrium result is in contrast to the BGK kinetic equation solution, which

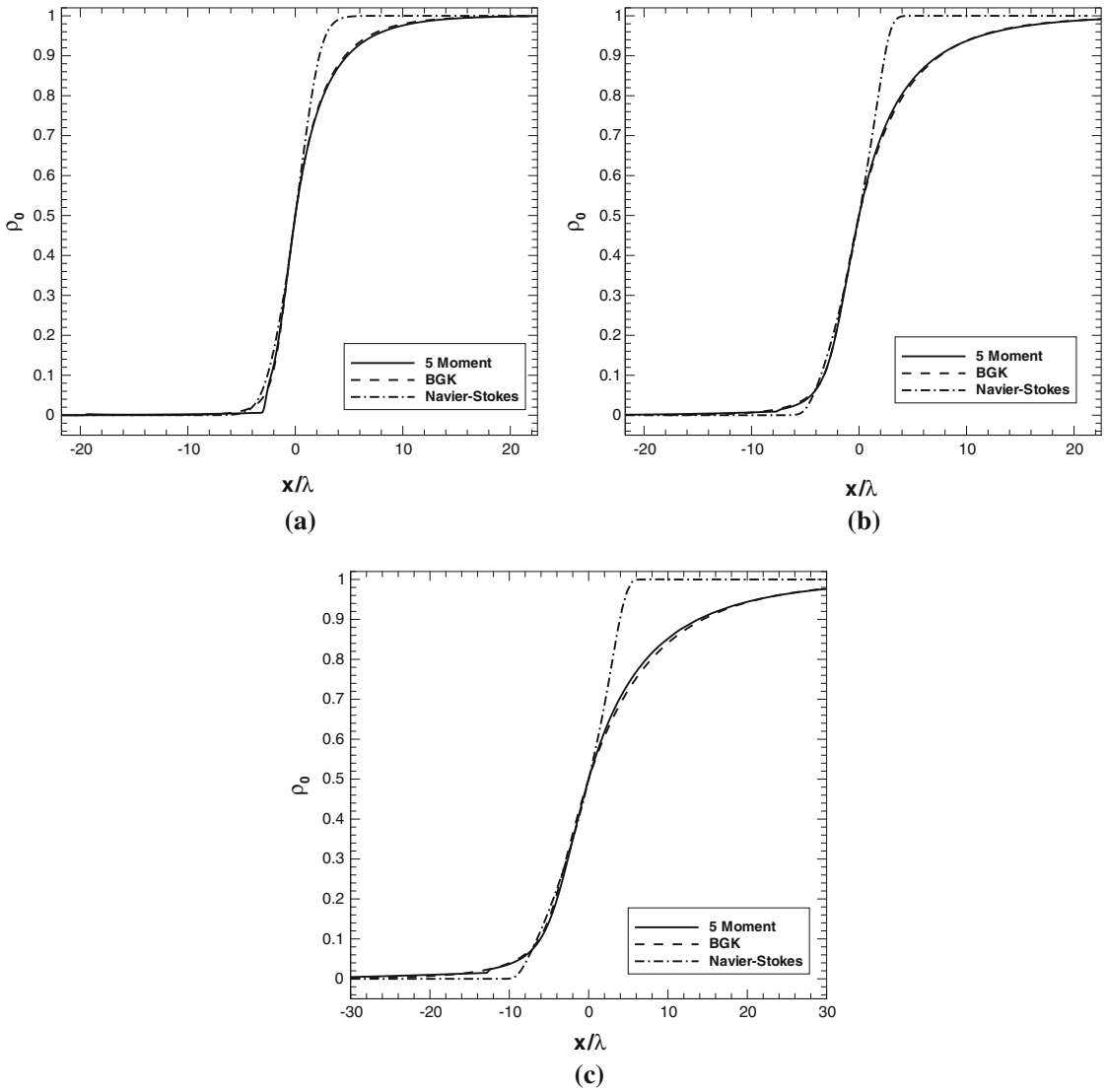


**Fig. 13** Predicted density distributions through a stationary shock wave for a one-dimensional gas as determined using the modified, realizable, 5-moment closure. The predicted shock structure is compared to results obtained by the direct numerical solution of the kinetic equation and "Navier–Stokes" equations for a range of shock Mach numbers, $M$: **a** $M = 2$; **b** $M = 4$; and **c** $M = 8$

consists of a single smooth transition between the two constant initial states, with no clearly identifiable wave structure. The agreement between 5-moment closure solution and the exact or BGK kinetic solution is certainly not very good in this case, indicating that, while it is still possible to obtain solutions, there is an upper bound on the Knudsen number for which the 5-moment model remains physically valid. Higher order moment closures would be needed to improve on this result. Note that, for this highly rarefied case, the time-step restriction for stability of the explicit time marching used in the solution of the equivalent "Navier–Stokes" equations, with its associated elliptic flux terms, made it difficult to carry out the simulations and results for the Navier–Stokes model are therefore not shown.

## 5 Conclusions

The current status of hyperbolic moment closures for the solution of continuum and non-equilibrium gaseous flows has been reviewed. Although possibly well established, the limitations of standard Grad and regularized Grad closures, in terms of closure breakdown and loss of hyperbolicity, has been described. Moreover, the

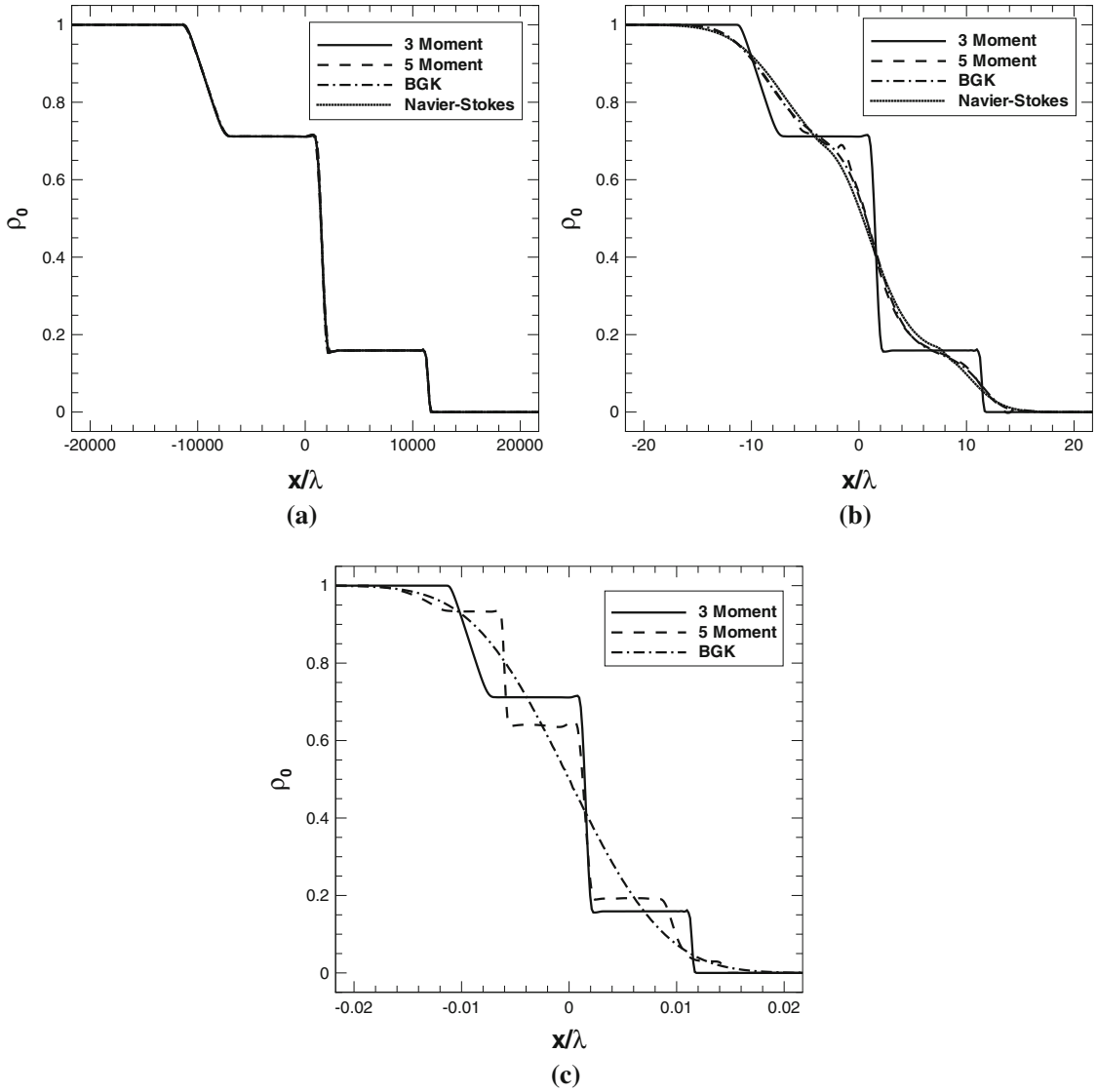


**Fig. 14** Predicted solutions for the Riemann initial value problem for a one-dimensional gas as determined using the modified, realizable, 5-moment closure. The predicted solutions of the Riemann problem are compared to those obtained for the equilibrium 3-moment closure, solutions obtained from the direct numerical solution of the kinetic equation, the "Navier–Stokes" solutions, and the 3-moment "Euler" solutions for a range of Knudsen numbers: **a** $Kn = 2.3 \times 10^{-5}$; **b** $Kn = 2.3 \times 10^{-2}$; and **c** $Kn = 23$

motivation for seeking a robust and purely hyperbolic description of non-equilibrium gaseous flow behavior has been established, both through theoretical discussions and through the application of the strictly hyperbolic and physically realizable Gaussian closure to a range of canonical flow problems. Although somewhat promising, the failure of the high-order members of maximum-entropy closures to remain valid for the full range of realizable moments is discussed. A modifications to the maximum-entropy closures of Levermore is then described that appears to result in valid closures for a wide range of physically realizable moments. The proposed modified closure has been applied to one-dimensional kinetic theory and promising numerical results were obtained. It seems possible to maintain a hyperbolic description for virtually the full range of physically realizable moments, although a formal proof of hyperbolicity remains illusive. Future research efforts will focus on the further investigation of the modified closures and the possible extension to fully three-dimensional kinetic theory.

**Acknowledgments** The authors would like to thank the two reviewers for their useful suggestions and comments, which have helped considerably to strengthen the analysis and results described above. This research was supported by the Natural Sciences and Engineering Research Council of Canada. Funding for the parallel computing facility used to perform the computations described herein was obtained from the Canadian Foundation for Innovation and Ontario Innovation Trust (CFI Project No. 2169). The authors are very grateful to these funding agencies for this support. The second author would also like to thank the Natural Science and Engineering Research Council of Canada for their generous support of his research through a Canadian Graduate Scholarship.

## References

1. O'Connor, L.: Mems: mircoelectromechanical systems. Mech. Eng. J. **114**(2), 40–47 (1992)
2. Meyyappan, M. (ed.): Computational Modeling in Semiconductor Processing. Artech House, Boston (1995)
3. Bird, G.A.: Molecular Gas Dynamics and the Direct Simulation of Gas Flows. Clarendon Press, Oxford (1994)
4. Mieussens, L.: Discrete velocity model and implicit scheme for the BGK equation of rarefied gas dynamics. Math. Models Methods Appl. Sci. **10**(8), 1121–1149 (2000)
5. Fan, J., Shen, C.: Statistical simulation of low-speed rarefied gas flow. J. Comput. Phys. **167**, 393–412 (2001)
6. Sun, Q., Boyd, I.D.: A direct simulation method for subsonic, mircoscale gas flow. J. Comput. Phys. **179**, 400–425 (2002)
7. Grad, H.: On the kinetic theory of rarefied gases. Commun. Pure Appl. Math. **2**, 331–407 (1949)
8. Levermore, C.D.: Moment closure hierarchies for kinetic theories. J. Stat. Phys. **83**, 1021–1065 (1996)
9. Müller, I., Ruggeri, T.: Rational Extended Thermodynamics. Springer, New York (1998)
10. Struchtrup, H.: Macroscopic Transport Equations for Rarefied Gas Flows. Springer, Berlin (2005)
11. Brown, S.L., Roe, P.L., Groth, C.P.T.: Numerical solution of a 10-moment model for nonequilibrium gasdynamics. Paper 95–1677, AIAA, June (1995)
12. Brown, S.L.: Approximate Riemann solvers for moment models of dilute gases. PhD thesis, University of Michigan (1996)
13. Godunov, S.K.: Finite-difference method for numerical computations of discontinuous solutions of the equations of fluid dynamics. Math. Sb. **47**, 271–306 (1959)
14. McDonald, J.G., Groth, C.P.T.: Numerical modeling of micron-scale flows using the Gaussian moment closure. Paper 2005-5035, AIAA, June 2005
15. Sachdev, J.S., Groth, C.P.T., Gottlieb J.J.: Parallel AMR scheme for turbulent multi-phase rocket motor core flows. Paper 2005–5334, AIAA, June 2005
16. Sachdev, J.S., Groth, C.P.T.: A mesh adjustment scheme for embedded boundaries. Commun. Computat. Phys. **2**(6), 1095–1124 (2007)
17. Sachdev, J.S.: Parallel solution-adaptive method for predicting solid propellant rocket motor core flows. PhD thesis, University of Toronto, April 2007
18. McDonald, J.G., Sachdev, J.S., Groth, C.P.T.: Gaussian moment closure for the modelling of continuum and micron-scale flows with moving boundaries. In: Proceedings of the Fourth International Conference on Computational Fluid Dynamics, ICCFD4, Ghent, Belgium, July 10–14, 2006. Heidelberg, to appear. Springer-Verlag
19. Struchtrup, H., Torrilhon, M.: Regularization of grad's 13 moment equations: Derivation and linear analysis. Phys. Fluids **15**, 2668–2680 (2003)
20. Struchtrup, H., Torrilhon, M.: H theorem, regularization, and boundary conditions for the linearized 13 moment equations. Phys. Rev. Lett. **99**, 014502 (2007)
21. Torrilhon, M., Struchtrup, H.: Boundary conditions for regularized 13 moment equations for micro-channel-flows. J. Comput. Phys. **227**, 1982–2011 (2008)
22. Coirier, W.J.: An adaptively-refined, Cartesian, cell-based scheme for the Euler and Navier–Stokes equations. PhD thesis, University of Michigan (1994)
23. Coirier, W.J., Powell, K.G.: Solution-adaptive Cartesian cell approach for viscous and inviscid flows. AIAA J. **34**(5), 938–945 (1996)
24. McDonald, J.G.: Numerical modeling of micron-scale flows using the Gaussian moment closure. Master's thesis, University of Toronto (2005)
25. Junk, M.: Domain of definition of levermore's five-moment system. J. Stat. Phys. **93**(5/6), 1143–1167 (1998)
26. Junk, M.: Maximum entropy moment systems and galilean invariance. Contin. Mech. Thermodyn. **14**, 563–576 (2002)
27. Schneider, J.: Entropic approximation in kinetic theory. Math. Model. Numer. Anal. **38**(3), 541–561 (2004)
28. Hauck, C.D., Levermore, C.D., Tits, A.L.: Convex duality and entropy-based moment closures: Characterizing degenerate densities. SIAM J. Control Opt. **47**(4), 1977–2015 (2008)
29. Chapman, S., Cowling, T.G.: The Mathematical Theory of Non-Uniform Gases. Cambridge University Press, Cambridge (1960)
30. Burgers, J.M.: Flow Equations for Composite Gases. Academic Press, New York (1969)
31. Hamburger, H.L.: Hermitian transformations of deficiency-index (1, 1), jacobian matrices, and undetermined moment problems. Am. J. Math. **66**, 489–552 (1944)
32. Reed, M., Simon, B.: Methods of Modern Mathematical Physics, II: Fourier Analysis, Self-Adjointness. Academic Press, New York (1975)
33. Godunov, S.K.: An interesting class of quasilinear systems. Sov. Math. Dokl. **2**, 947–949 (1961)
34. Friedrichs, K.O., Lax, P.D.: Systems of conservation laws with a convex extension. ProcNAS **68**, 1686–1688 (1971)
35. Maxwell, J.C.: On the dynamical theory of gases. Philos. Trans. R. Soc. Lond. **157**, 49–88 (1867)
36. Hertweck, F.: Allgemeine 13-momenten-näherung zur fokker-planck-gleichung eines plasmas. Z. Naturforsch. **20**, 1243–1255 (1965)
37. Oraevskii, V., Chodura, R., Feneberg, W.: Hydrodynamic equations for plasmas in strong magnetic fields—i collisionless approximation. Plasma Phys. **10**, 819–828 (1968)

38. Holway, L.H.: Approximation procedures for kinetic theory. PhD thesis, Harvard University (1963)
39. Holway, L.H.: Kinetic theory of shock structure using an ellipsoidal distribution function. In: de Leeuw, J.H. (ed.) Rarefied Gas Dynamics, vol. I, pp. 193–215. Academic Press, New York (1966)
40. Holway, L.H.: New statistical models for kinetic theory: Methods of construction. Phys. Fluids **9**(9), 1658–1673 (1966)
41. Holway, L.H.: The effect of collisional models upon shock wave structure. In: Brundin, C.L. (ed.) Rarefied Gas Dynamics, vol. I, pp. 759–784. Academic Press, New York (1967)
42. Bhatnagar, P.L., Gross, E.P., Krook, M.: A model for collision processes in gases. i. small amplitude processes in charged and neutral one-component systems. Phys. Rev. **94**(3), 511–525 (1954)
43. Hittinger, J.A.: Foundations for the generalization of the Godunov method to hyperbolic systems with stiff relaxation source terms. PhD thesis, University of Michigan (2000)
44. McDonald, J.G., Groth, C.P.T.: Extended fluid-dynamic model for micron-scale flows based on gaussian moment closure. Paper 2008–0691, AIAA, January 2008
45. Kennard, E.H.: Kinetic Theory of Gases. McGraw-Hill, New York (1938)
46. Khieu, L., van Leer, B., Suzuki, Y.: An analysis of a space-time discontinous-galerkin method for moment equations and its solid-boundary treatment. Paper 2009–3874, AIAA, June 2009
47. Thomas, P.D., Lombard, C.K.: Geometric conservation laws and its application to flow computations on moving grids. AIAA J. **17**(10), 1030–1037 (1979)
48. Barth, T.J.: Recent developments in high order k-exact reconstruction on unstructured meshes. Paper 93–0668, AIAA, January 1993
49. Venkatakrishnan, V.: On the accuracy of limiters and convergence to steady state solutions. Paper 93–0880, AIAA, January 1993
50. Roe, P.L.: Approximate Riemann solvers, parameter vectors, and difference schemes. J. Comput. Phys. **43**, 357–372 (1981)
51. Osher, S., Fedkiw, R.: Level Set Methods and Dynamic Implicit Surfaces, volume 153 of Applied Mathematical Sciences. Springer, New York (2003)
52. Sethian, J.A.: Level Set Methods and Fast Marching Methods. Cambridge Monographs on Applied and Computational Mathematics, 2nd edn. Cambridge University Press, Cambridge (1999)
53. Vincenti, W.G., Kruger, C.H.: Introduction to Physical Gas Dynamics. R. E. Krieger Publishing, Huntington, NY (1975)
54. Trepaud, P., Coudeville, H., Brun, E.A.: Drag measurements in slip and transition flow. In: Proceedings of the Fourth International Symposium on Rarefied Gas Dynamics. Academic Press, New York (1965)
55. Patterson, G.N.: Introduction to the Kinetic Theory of Gas Flows. University of Toronto Press, Toronto (1961)
56. Williamson, C.H.K.: Oblique and parallel modes of vortex shedding in the wake of a circular cylinder at low reynolds numbers. J. Fluid Mech. **206**, 579–627 (1989)
57. Braza, M., Chassaing, P., Ha Minh, H.: Numerical study and physical analysis of the pressure and velocity fields in the near wake of a circular cylinder. J. Fluid Mech. **165**, 79–130 (1986)
58. Schlichting, H.: Boundary-Layer Theory, 7th edn. McGraw-Hill, Toronto (1979)
59. Allegre, J., Raffin, M., Lengrand, J.C.: Experimental flowfields around NACA0012 airfoils located in subsonic and supersonic rarefied air streams. In: Bristeau, M.O., Glowinski, R., Periaux, J. Viviand, H. (eds.) Numerical Simulation of Compressible Navier–Stokes Flows, vol. 18 of Notes on Numerical Fluid Dynamics. Fried. Vieweg and Sohn, Braunschweig, Germany, pp. 59–68 (1987)
60. Suzuki, Y., van Leer, B.: Application of the 10-moment model to MEMS flows. Paper 2005–1398, AIAA, January (2005)
61. Au, J.D.: Lösung Nichtlinearer Problems in der Erweiterten Thermodynamik. PhD thesis, Technische Universität Berlin (2001)
62. Harten, A., Lax, P.D., van Leer, B.: On upstream differencing and Godunov-type schemes for hyperbolic conservation laws. SIAM Rev. **25**(1), 35–61 (1983)